Neuron

Article

VTA Glutamatergic Neurons Mediate Innate Defensive Behaviors

Graphical Abstract

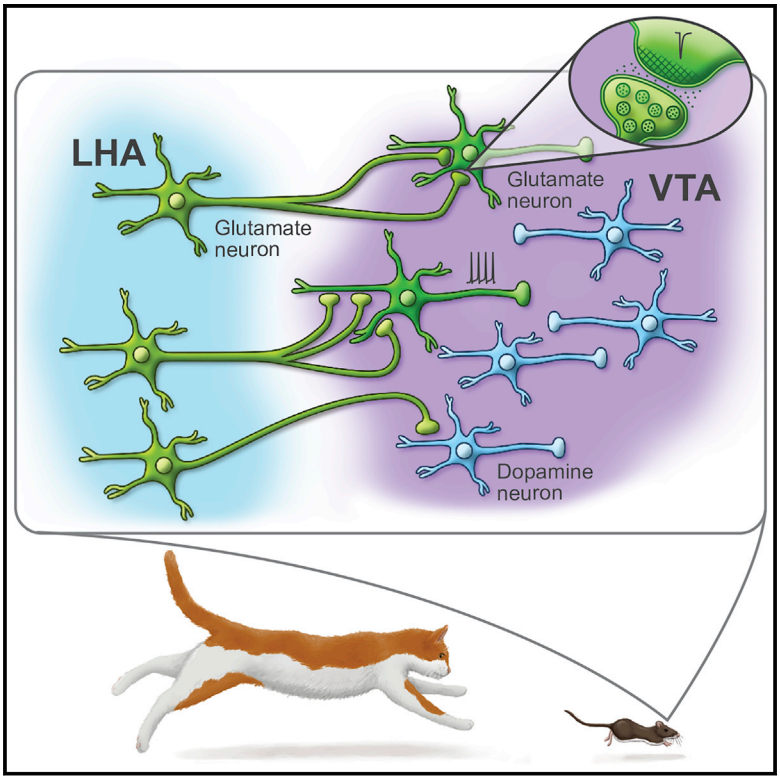

Authors

M. Flavia Barbano, Hui-Ling Wang, Shiliang Zhang, ..., Bing Liu, David J. Barker, Marisela Morales

Correspondence

mmorales@intra.nida.nih.gov

In Brief

Innate defensive behaviors are unlearned responses, evolutionarily selected to increase chances of survival. Here, Barbano et al. report that ventral tegmental area glutamatergic neurons are activated by and required for innate defensive responses and that information on threatening stimuli to these glutamate neurons is relayed by hypothalamic excitatory neurons.

Highlights

- Ventral tegmental area (VTA)-glutamate neurons encode innate defensive behavior
- A single VTA-glutamate neuron receives multiple hypothalamic excitatory inputs
- Hypothalamic excitatory inputs to VTA-glutamate neurons convey treating information

Barbano et al., 2020, Neuron *107*, 1–15
July 22, 2020 Published by Elsevier Inc.
https://doi.org/10.1016/j.neuron.2020.04.024

CellPress

Please cite this article in press as: Barbano et al., VTA Glutamatergic Neurons Mediate Innate Defensive Behaviors, Neuron (2020), https://doi.org/10.1016/j.neuron.2020.04.024

Neuron

CellPress

Article

VTA Glutamatergic Neurons Mediate Innate Defensive Behaviors

M. Flavia Barbano,[1] Hui-Ling Wang,[1] Shiliang Zhang,[2] Jorge Miranda-Barrientos,[1] David J. Estrin,[1] Almaris Figueroa-González,[1] Bing Liu,[1] David J. Barker,[3] and Marisela Morales[1,4,*]

[1]Integrative Neuroscience Research Branch, National Institute on Drug Abuse, Baltimore, MD 21224, USA
[2]Confocal and Electron Microscopy Core, National Institute on Drug Abuse, Baltimore, MD 21224, USA
[3]Department of Psychology, Rutgers the State University of New Jersey, Piscataway, NJ 08854, USA
[4]Lead Contact
*Correspondence: mmorales@intra.nida.nih.gov
https://doi.org/10.1016/j.neuron.2020.04.024

SUMMARY

The ventral tegmental area (VTA) has dopamine, GABA, and glutamate neurons, which have been implicated in reward and aversion. Here, we determined whether VTA-glutamate or -GABA neurons play a role in innate defensive behavior. By VTA cell-type-specific genetic ablation, we found that ablation of glutamate, but not GABA, neurons abolishes escape behavior in response to threatening stimuli. We found that escape behavior is also decreased by chemogenetic inhibition of VTA-glutamate neurons and detected increases in activity in VTA-glutamate neurons in response to the threatening stimuli. By ultrastructural and electrophysiological analysis, we established that VTA-glutamate neurons receive a major monosynaptic glutamatergic input from the lateral hypothalamic area (LHA) and found that photoinhibition of this input decreases escape responses to threatening stimuli. These findings indicate that VTA-glutamate neurons are activated by and required for innate defensive responses and that information on threatening stimuli to VTA-glutamate neurons is relayed by LHA-glutamate neurons.

INTRODUCTION

Defensive behaviors are characterized by different and often non-overlapping responses, such as freezing, fighting, or escape (Eilam, 2005; LeDoux and Daw, 2018; Mongeau et al., 2003). The selection of an adequate strategy to cope with a life-threatening situation is determined by the proximity or imminence of the threat, and it is vital for the survival of the individual and the species. Several brain areas have been implicated in defensive responses, including periaqueductal gray (Deng et al., 2016; Gross and Canteras, 2012; LeDoux and Daw, 2018; Li et al., 2018), amygdala (Gross and Canteras, 2012; LeDoux and Daw, 2018), hypothalamus (Gross and Canteras, 2012; Li et al., 2018; Mongeau et al., 2003; Wang et al., 2015a), and ventral tegmental area (VTA) (Wilson and Hall, 1988; Zhou et al., 2019).

The VTA has diverse cell types with distinct cytoarchitecture, connectivity, and function (Morales and Margolis, 2017), which includes dopamine neurons (expressing tyrosine hydroxylase [TH]) intermingled with glutamate (expressing vesicular glutamate transporter 2 [VGluT2]) and GABA (expressing vesicular GABA transporter [VGaT]) neurons. In addition, some VTA neurons co-release several neurotransmitters, either from the same or from different synaptic compartments (Berrios et al., 2016; Morales and Margolis, 2017; Root et al., 2014a; Zhang et al., 2015). VTA-dopamine neurons have been classically proposed to mediate reward processes (Berridge and Robinson, 1998; Schultz, 2016; Wise, 2004). However, VTA-dopamine neurons have also been implicated in signaling aversive stimuli (Brischoux et al., 2009; Bromberg-Martin et al., 2010; Lammel et al., 2014). Electrophysiological recordings in monkeys (Fiorillo et al., 2013) and mice (Matsumoto et al., 2016; Moriya et al., 2018) have shown an increased excitation of VTA-dopamine neurons in response to aversive stimuli, and calcium imaging studies have suggested a role of VTA-dopamine neurons projecting specifically to the ventromedial part of the nucleus accumbens (nAcc) shell in encoding aversive stimuli and the cues signaling those stimuli (de Jong et al., 2019).

In addition to VTA-dopamine neurons, both VTA-GABA and VTA-glutamate neurons have been shown to play a role in mediating aversion. Initial optogenetic studies demonstrated that VTA photoactivation of GABA neurons induces avoidance behavior by inhibiting neighboring dopamine neurons (Tan et al., 2012). In a more recent circuit-based study, it was demonstrated that place avoidance mediated by VTA-GABA neurons is regulated by lateral hypothalamus (LH) glutamatergic inputs, and activation of these inputs results in the suppression of dopamine release in nAcc (Nieh et al., 2016). We had previously shown that nAcc photoactivation of VTA-VGluT2 inputs drives aversion by a mechanism in which glutamate release from VTA-VGluT2 inputs induces the firing of local parvalbumin GABA-interneurons,

Please cite this article in press as: Barbano et al., VTA Glutamatergic Neurons Mediate Innate Defensive Behaviors, Neuron (2020), https://doi.org/10.1016/j.neuron.2020.04.024

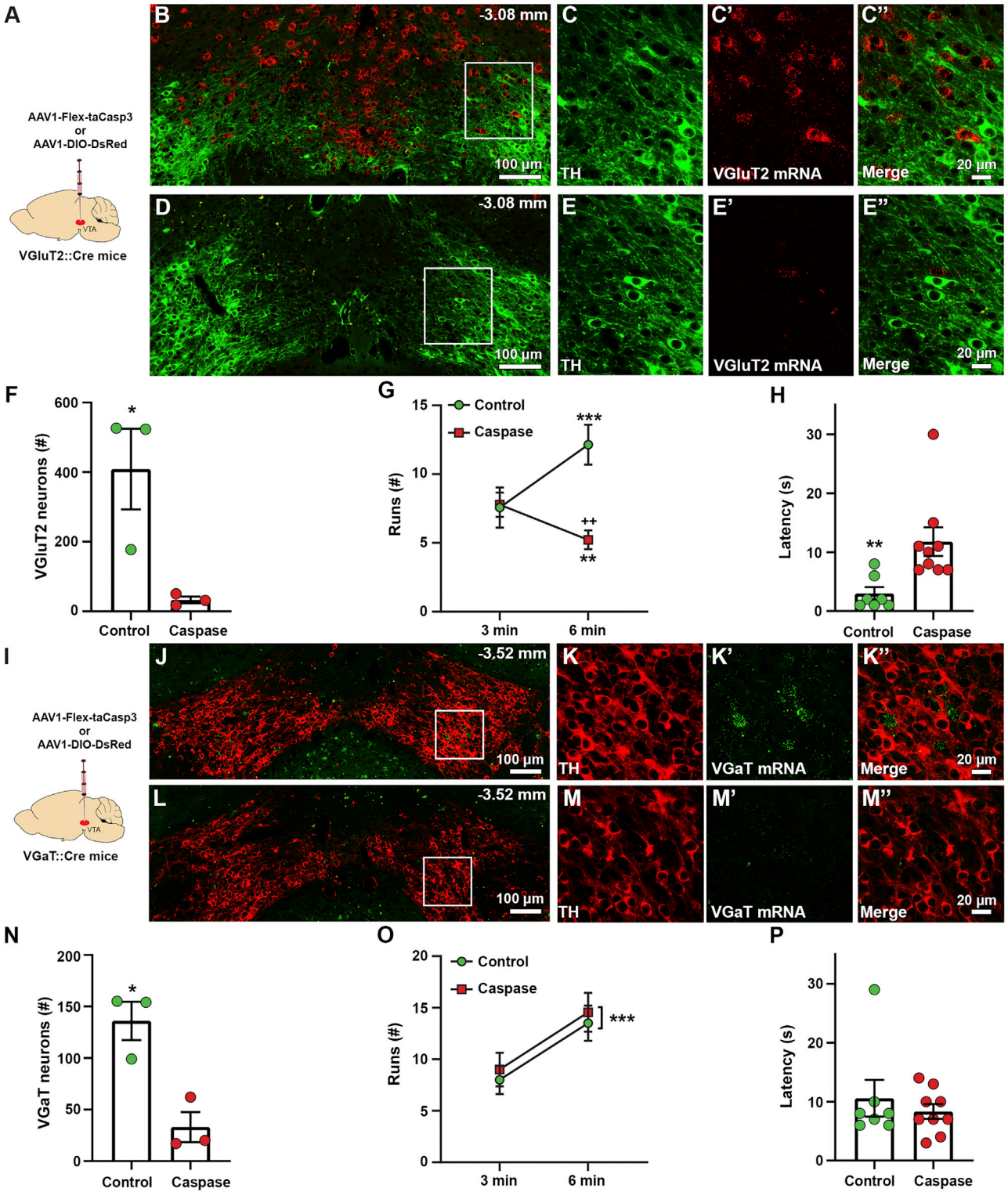

Figure 1. VTA-VGluT2 Neurons, but Not VGaT Neurons, Mediate Innate Escape Responses

(A) VTA viral injections.

(B–C'') Low (B) and high (C–C'') magnification of VTA from a control mouse (injected with AAV1-DIO-DsRed) showing neurons expressing VGluT2 mRNA (red) intermixed with TH-immunoreactive neurons (TH-IRs; green).

(legend continued on next page)

Please cite this article in press as: Barbano et al., VTA Glutamatergic Neurons Mediate Innate Defensive Behaviors, Neuron (2020), https://doi.org/10.1016/j.neuron.2020.04.024

resulting in inhibition of neighboring nAcc medium spiny neurons (Qi et al., 2016). Likewise, aversion is also promoted by lateral habenula photoactivation of VTA-VGluT2 inputs (Root et al., 2014b). Furthermore, we have recently shown by *in vivo* recordings that the firing rate of a large subpopulation of VTA-VGluT2 neurons increases in response to aversive stimuli (Root et al., 2018). Here, we determined whether VTA-VGluT2 and VTA-GABA neurons play a role in innate defensive responses.

RESULTS

VTA-VGluT2 Neurons, but Not VTA-VGaT Neurons, Mediate Innate Escape Responses

To examine the role of VTA-VGluT2 neurons in innate escape behavior, we expressed the apoptosis-inducing protein, caspase-3 (Casp3) in VTA-VGluT2 neurons in VGluT2::Cre mice (Figure 1A). By RNAscope VTA cellular detection of VGluT2 mRNA, we confirmed the ablation of VTA-VGluT2 neurons (Figures 1B–1F). By testing VTA-VGluT2 ablated and control mice responses to a looming stimulus (a black disc mechanically descended above the open field arena, mimicking an aerial predator attack; De Franceschi et al., 2016; Evans et al., 2018; Huang et al., 2017; Wei et al., 2015; Zhou et al., 2019), we found that control mice displayed more runs in response to the threatening stimulus than in its absence (12.1 ± 1.5 versus 7.6 ± 1.5; Figure 1G), contrasting with fewer runs in VTA-VGluT2 ablated mice (baseline, 7.8 ± 0.9; looming, 5.2 ± 0.7; Figure 1G). In a second test, we measured escape latency to exposure of the synthetic predator odor trimethylthiazoline (10% TMT; Rosen et al., 2015) and found a shorter escape latency (3.0 ± 1.1; Figure 1H) in control mice than in VTA-VGluT2 ablated mice (11.8 ± 2.4; Figure 1H). Locomotor activity was not affected by ablation of VTA-VGluT2 neurons (Figures S1A–S1C). These findings suggest a role of VTA-VGluT2 neurons in innate escape behaviors.

Given that previous studies have shown a role in aversion by VTA-GABA neurons (Tan et al., 2012; Nieh et al., 2016), we examined the possible contribution of these neurons in innate escape behavior. As for VTA-VGluT2 neuronal ablation, we genetically ablated VTA-GABA neurons by Casp3 expression into the VTA of VGaT::Cre mice (Figure 1I) and by RNAscope detection of VGaT mRNA confirmed their ablation (Figures 1J–1N). We found that both control and VTA-VGaT ablated mice showed similar number of runs in response to looming stimulus (Figure 1O) and similar escape latencies in response to TMT exposure (Figure 1P), without affecting locomotor activity (Figures S1D–S1F). These results indicate that, in contrast to VTA-VGluT2 neurons, VTA-VGaT neurons do not seem to be involved in escape behavior in response to looming or odor-threatening stimuli.

VTA-VGluT2 Neurons Encode Innate Escape Responses

By *in vivo* fiber photometry, we tested the participation of VTA-VGluT2 neurons in innate escape behavior. We expressed GCaMP6s in VTA-VGluT2 neurons of VGluT2::Cre mice and recorded Ca^{2+} activity in VTA-VGluT2 neurons in response to a looming stimulus (Figures 2A and S2A–S2C). We detected significant increases in Ca^{2+} activity in VTA-VGluT2 neurons in response to a looming stimulus when compared with pre-stimulus baseline (Figures 2B and 2C). We observed that these increases in Ca^{2+} activity in VTA-VGluT2 neurons were long lasting (Figures 2B and 2C), suggesting that they were not just reflecting responses to sensory events. Given that there is the possibility that increases in Ca^{2+} activity in VTA-VGluT2 neurons in response to the looming stimulus may reflect responses to visual events, we next recorded Ca^{2+} activity in VTA-VGluT2 neurons in response to both a neutral odor (10% lemon odor) and to TMT odor (10%; Figures 2D–2F). Although both odors increased Ca^{2+} activity in VTA-VGluT2 neurons, the increases were greater in response to TMT (Figures 2E and 2F), suggesting that VTA-VGluT2 neurons were tuned to the threatening stimuli.

By *in vivo* recordings, we have shown that some VTA-VGluT2 neurons increase their firing rate in response to sucrose delivery (Root et al., 2018), raising the possibility that different subpopulations of VTA-VGluT2 neurons respond differentially to appetitive or aversive stimuli. To test this possibility, we recorded Ca^{2+} activity in VTA-VGluT2 neurons while mice were eating standard chow or palatable sucrose pellets (Figures S2C and S2G). Although we observed increases in Ca^{2+} activity for both foods, the responses were not significantly different from

(D–E'') Low (D) and high (E–E'') magnification of VTA from a mouse injected with AAV1-Flex-taCasp3 showing TH-IRs and lack of VGluT2 mRNA.
(F) VTA-VGluT2 neurons are present in control mice (408.67 ± 115.84; 3 mice) but infrequent in caspase mice (32.67 ± 9.56; 3 mice; 3 sections per mouse; $t_{(4)} = -3.23$, *p < 0.05, t test; data represent mean ± SEM).
(G) Number of runs induced by looming stimulus is lower in caspase mice than in control mice (control, n = 7; caspase, n = 9; group × experimental phase: $F_{(1,14)} = 56.07$, p < 0.001, ANOVA with Newman-Keuls post hoc test; data represent mean ± SEM). **p < 0.01 and ***p < 0.001 against the first 3 min of the test for each group; ++p < 0.01 against control.
(H) Escape latency from TMT odor is higher in caspase mice than in control mice (control, n = 7; caspase, n = 9; $t_{(14)} = -2.98$, **p < 0.01, t test; data represent mean ± SEM).
(I) VTA viral injections.
(J–K'') Low (J) and high (K–K'') magnification of VTA from a control mouse (injected with AAV1-DIO-DsRed) showing neurons expressing VGaT mRNA (green) intermixed with TH-IR cells (red).
(L–M'') Low (L) and high (M–M'') magnification of VTA from a mouse injected with AAV1-Flex-taCasp3 showing TH-IRs and lacking VGaT mRNA.
(N) VTA-VGaT neurons are present in control mice (136 ± 18.5; 3 mice) but infrequent in caspase mice (33 ± 14.53; 3 mice; 3 sections per mouse; $t_{(4)} = 4.38$, *p < 0.05, t test; data represent mean ± SEM).
(O) The number of runs induced by looming stimulus is similar in control and caspase mice (control, n = 7; caspase, n = 9; group × experimental phase: $F_{(1,14)} = 0.002$, p = 0.97, ANOVA; ***p < 0.001 against the first 3 min of the experiment; data represent mean ± SEM).
(P) The latency to escape from TMT odor is similar in control and caspase mice (control, n = 7; caspase, n = 9; $t_{(14)} = 0.73$, p = 0.48, t test; data represent mean ± SEM).
See also Figure S1.

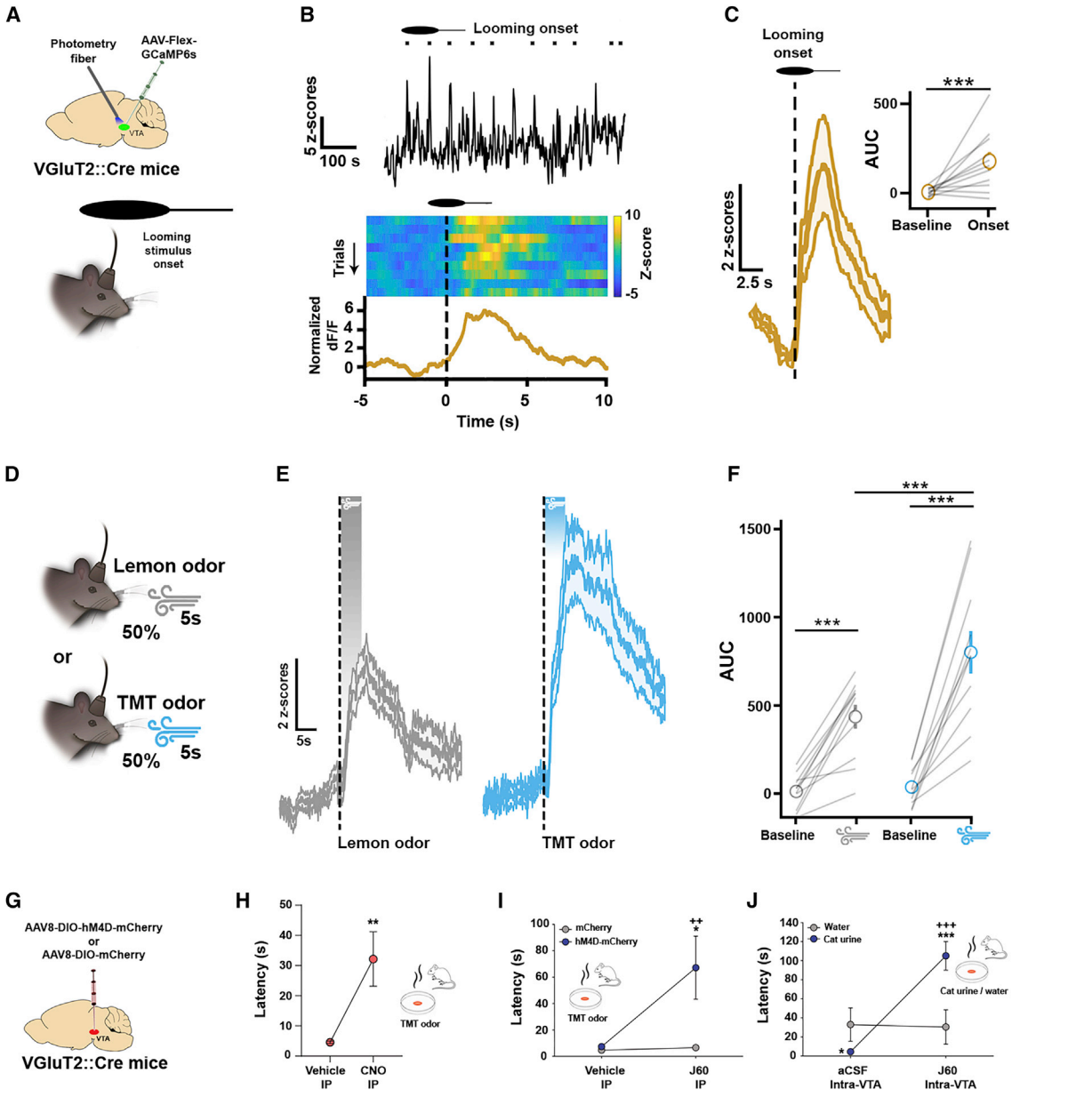

Figure 2. VTA-VGluT2 Neurons Encode Innate Escape Responses

(A) VTA viral injection of AAV-Flex-GCaMP6s and VTA photometry fiber (top); schematic representation of the looming stimulus (bottom).

(B) Whole session recording from VTA-VGluT2 neurons showing time of looming stimulus onset (top); heatmap of Ca^{2+} activity over successive looming trials (middle); cell population responses to looming stimulus onset showing increases in Ca^{2+} activity in VTA-VGluT2 neurons (bottom).

(C) Population Ca^{2+}activity (±SEM) in VTA-VGluT2 neurons during looming stimulus onset. Inset: area under the curve (AUC) for Ca^{2+} activity in VTA-VGluT2 neurons before (−5 to 0 s, baseline) and after (0–5 s, onset) onset of looming stimulus is shown (n = 12; t test; $t_{(186)} = 6.52$, ***p < 0.001; data represent mean ± SEM).

(D) Schematic representation of odor exposure.

(E) Population of Ca^{2+} activity (±SEM) in VTA-VGluT2 neurons in response to lemon (left) or TMT (right) odor.

(F) AUC for Ca^{2+} activity in VTA-VGluT2 neurons in response to lemon or TMT odors (n = 12; odor × epoch: $F_{(1,426)} = 9.50$, p < 0.001, ANOVA with Bonferroni post hoc test; ***p < 0.001; data represent mean ± SEM).

(G) Viral injections of AAV-hM4D-mCherry or AAV-mCherry in VTA of VGluT2::Cre mice.

(H) Chemogenetic inhibition of VTA-VGluT2 neurons by intraperitoneal (IP) CNO injection (3 mg/kg) increased escape latency from TMT odor ($t_{(25)} = -27.61$, p = 0.005, t test; data represent mean ± SEM). ++p < 0.01 against vehicle.

(legend continued on next page)

Please cite this article in press as: Barbano et al., VTA Glutamatergic Neurons Mediate Innate Defensive Behaviors, Neuron (2020), https://doi.org/10.1016/j.neuron.2020.04.024

baseline (Figures S2H–S2J). In the same experiment, we next recorded Ca^{2+} activity while lightly grabbing mice from the tail and lifting them from the ground, a condition in which mice display escape responses. We detected significant increases in Ca^{2+} activity in response to mouse lift, suggesting that VTA-VGluT2 neurons' response is greater to threatening versus appetitive stimuli (Figures S2H–S2K).

To determine a causal role for VTA-VGluT2 neurons in innate escape behavior, we studied TMT-induced escape behavior in mice expressing hM4D (inhibitory Gi-coupled designer receptors exclusively activated by designer drugs [DREADDs]) in VTA-VGluT2 neurons (Figures 2G, S2D, and S2E). We found that VTA-VGluT2 neuronal chemogenetic inactivation by peripheral injection of the hM4D ligands clozapine-N-oxide (CNO) (Figure 2H) or JHU 37160 (J60; Figure 2I) increased the escape latency to TMT odor presentation when compared with vehicle injection. We did not observe changes in mice locomotor activity induced by CNO or J60 (Figures S2F and S2L). In another set of mice expressing hM4D-mCherry in VTA-VGluT2 neurons, we examined effects of intra-VTA injections of artificial cerebrospinal fluid (aCSF) or J60 in response to cat litter containing either water or cat urine. We observed that, when mice received intra-VTA aCSF injections, they escaped faster when presented with cat urine than when presented with water, but intra-VTA J60 injections significantly increased cat-urine-induced escape latency, without affecting the response to water presentation (Figures 2J and S2M). These findings from chemogenetic inhibition indicate that VTA-VGluT2 neurons mediate innate escape behaviors.

A Major Monosynaptic Glutamatergic Input to VTA-VGluT2 Neurons from Lateral Hypothalamic Area (LHA)

We next looked for possible sources of glutamatergic synaptic inputs to induce activation of VTA-VGluT2 neurons. Tracing studies have shown that LH-VGluT2 neurons provide a major glutamatergic input to VTA (Geisler et al., 2007), and rabies-virus-based *trans*-synaptic retrograde tracing studies have suggested that LH provides a major monosynaptic input to VTA-VGluT2 neurons (Faget et al., 2016; Beier et al., 2019). Thus, we next determine the extent to which monosynaptic inputs to VTA-VGluT2 neurons derived from LHA-VGluT2 neurons. By VTA injection of retrograde tract tracer Fluoro-Gold (FG) (Figure S3A), we found the highest concentration of FG neurons within LHA (349.3 ± 91.5 neurons), fewer FG neurons in neighboring ventromedial hypothalamic nucleus (2.0 ± 1.0 neurons), anterior hypothalamic area (anterior part; 2.3 ± 1.2 neurons), anterior hypothalamic area (posterior part; 8.0 ± 3.2 neurons), paraventricular hypothalamic nucleus (ventral part; 21.3 ± 9.3 neurons), dorsomedial hypothalamic nucleus (42.7 ± 11.0 neurons), and posterior hypothalamic area (77.3 ± 27.7 neurons; Figures S3F, S3G, and S3I). By *in situ* hybridization (Figures S3B–S3E″), we found that, within the total population of LHA FG neurons, ≈40% (40.3% ± 2.3%; 466/1,231 FG neurons) co-expressed VGluT2 mRNA and ≈60% (59.7% ± 2.3%; 765/1,231 FG neurons) lacked VGluT2 mRNA (Figure S3H). Although we observed FG neurons co-expressing VGluT2 mRNA throughout rostral (−1.22 bregma), medial (−1.58 bregma), and caudal (−1.94 bregma) aspects of the LHA (Figure S3J), FG neurons lacking VGluT2 mRNA were concentrated in medial and caudal aspects of the LHA (Table S1). These findings indicate that VTA receives a major input from LHA-VGluT2 neurons.

Next, we determined the extent to which LHA-VGluT2 neurons synapse on VTA-VGluT2 neurons in mice that expressed mCherry in LHA-VGluT2 neurons and eYFP in VTA-VGluT2 neurons (Figure 3A). We confirmed the distribution of VGluT2 neurons expressing mCherry in LHA perifornical area (Figures S4A–S4E), identified in VTA mCherry axons intermixed with VGluT2-eYFP neurons (Figures 3B and 3C), and determined that mCherry-axon terminals co-expressed VGluT2-protein (Figure 3C). By ultrastructural analysis, we found that, from the total population of LHA-VGluT2-mCherry-axon terminals establishing synapses, 46.6% ± 4.2% made asymmetric synapses on both dendrites and soma of VTA-VGluT2-eYFP neurons (n = 1,420 terminals; Figures 3D–3K, S5A, S5C, and S5C′). Moreover, we determined that multiple LHA-VGluT2-mCherry-axon terminals established synapses on a single VTA-VGluT2-eYFP dendrite (Figure 3D). These ultrastructural synaptic findings indicate that LHA-VGluT2 neurons provide a major excitatory regulation on single VTA-VGluT2 neurons.

By ultrastructural analysis, we also examined the synaptic connectivity of LHA-VGluT2 axon terminals on VTA-TH neurons and found that, from the total population of LHA-VGluT2-mCherry axon terminals establishing synapses, 31.5% ± 3.3% made asymmetric synapses on TH-dendrites (n = 1,690 terminals; Figures 3K and S5B). Although we did not detect LHA-VGluT2-mCherry terminals making synapses on somas containing only TH, we detected LHA-VGluT2-mCherry terminals making synapses on somas of VGluT2 neurons co-expressing TH (Figure 3C). The ultrastructural synaptic findings showing that LHA-VGluT2 neurons establish multiple synapses on single VTA-VGluT2 dendrites and somas but few synapses on single VTA-TH dendrites and never on somas of TH-only neurons indicate that glutamate release from LHA-VGluT2 fibers has a stronger excitatory influence on VTA-VGluT2 neurons than on VTA-dopamine-only neurons.

To further confirm the monosynaptic excitatory nature of the synapses established by LHA-VGluT2 terminals on VTA-VGluT2 neurons, we prepared VTA slices from mice expressing eYFP in local VGluT2 neurons and mCherry in fibers from LHA-VGluT2 neurons. By voltage clamp recordings of VTA-VGluT2-eYFP

(I) Chemogenetic inhibition of VTA-VGluT2 neurons by IP J60 injection (0.1 mg/kg) increased escape latency from TMT odor (mCherry: n = 6; hM4D-mCherry: n = 6; group × treatment: $F_{(1,10)} = 5.61$; $p < 0.05$, ANOVA with Newman-Keuls post hoc test; data represent mean ± SEM). *$p < 0.05$ against vehicle; ++$p < 0.01$ against mCherry.

(J) Chemogenetic inhibition of VTA-VGluT2 neurons by intra-VTA J60 injection (0.1 μg/μL) increased escape latency from cat urine odor (hM4D-mCherry: n = 6; odor × treatment: $F_{(1,5)} = 51.31$; $p < 0.001$, ANOVA with Newman-Keuls post hoc test; data represent mean ± SEM). *$p < 0.05$; ***$p < 0.001$ against water odor; +++$p < 0.001$ against aCSF.

See also Figure S2.

Please cite this article in press as: Barbano et al., VTA Glutamatergic Neurons Mediate Innate Defensive Behaviors, Neuron (2020), https://doi.org/10.1016/j.neuron.2020.04.024

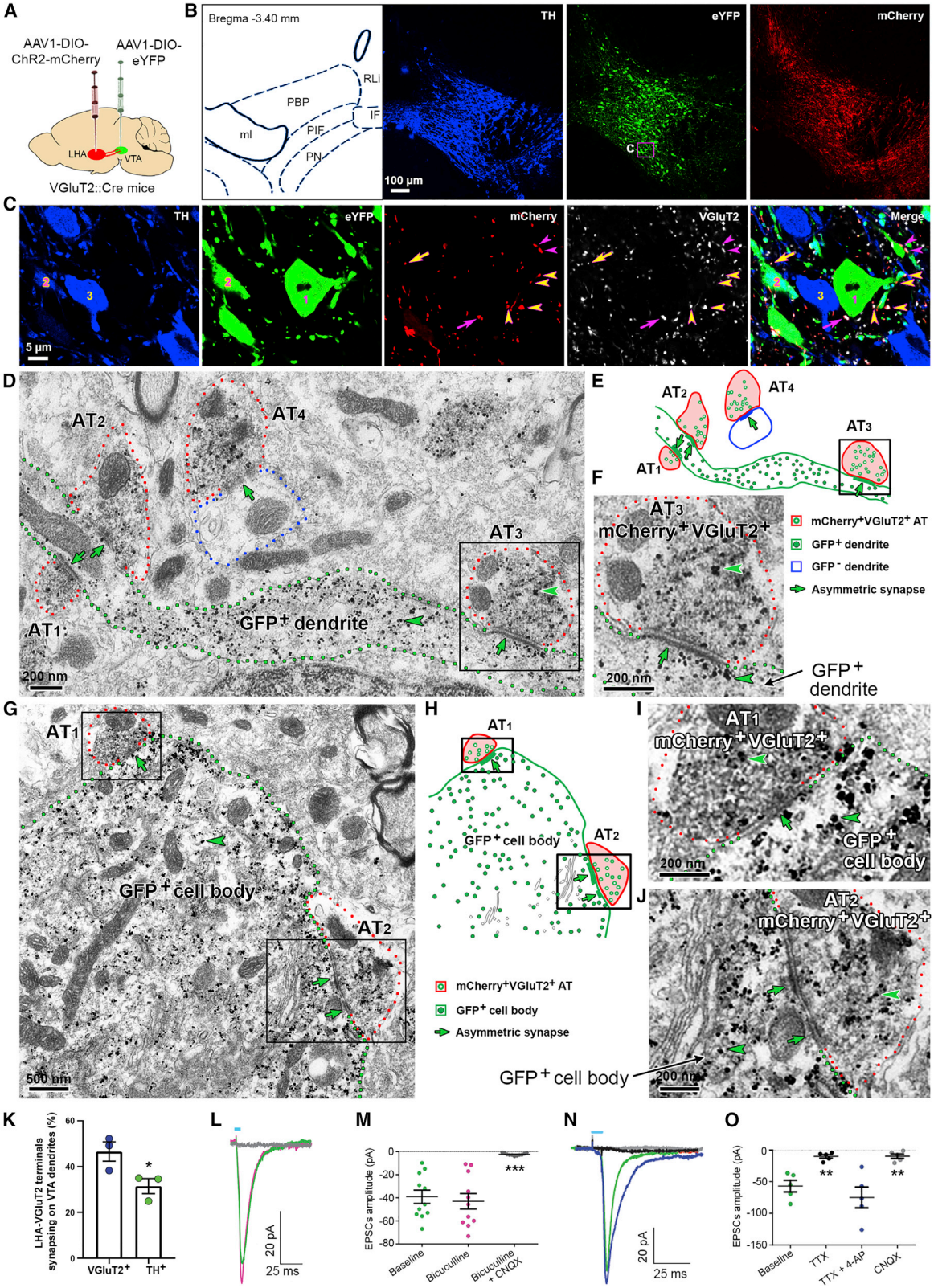

(legend on next page)

Please cite this article in press as: Barbano et al., VTA Glutamatergic Neurons Mediate Innate Defensive Behaviors, Neuron (2020), https://doi.org/10.1016/j.neuron.2020.04.024

neurons, we detected excitatory postsynaptic currents (EPSCs) evoked by photoactivation of LHA-VGluT2-mCherry fibers (Figure 3L). The amplitude of the EPSCs was not significantly affected by bath application of $GABA_A$ receptor antagonist bicuculline, but it was abolished by AMPA receptor antagonist CNQX (Figures 3L–3O). EPSCs amplitude was also blocked by bath application of tetrodotoxin (Figures 3N and 3O) and restored by 4-aminopyridine (Figures 3N and 3O), demonstrating monosynaptic glutamatergic transmission from LHA-VGluT2 fibers to VTA-VGluT2 neurons. In current clamp recordings, we detected a single action potential firing in VTA-VGluT2-eYFP neurons in response to a single pulse of photoactivation of LHA-VGluT2 fibers (Figure S5D) and observed burst firing in VTA-VGluT2 neurons in response to repetitive 20-Hz, 1-s photostimulation of LHA-VGluT2 fibers (Figure S5E). These findings indicate that VTA release of glutamate from LHA-VGluT2 fibers drives the firing of VTA-VGluT2 neurons via activation of their glutamatergic receptors.

We next determined the extent to which activation of LHA-VGluT2 inputs induced VTA expression of c-Fos (a marker of neuronal activation) in mice with LHA-VGluT2 neuronal expression of ChR2-eYFP (ChR2-eYFP mice; Figures S6A and S6B) or eYFP (eYFP mice; Figures S6A–S6F). After VTA photostimulation, we detected 2.5 times more c-Fos neurons in the VTA of ChR2-eYFP mice (279.7 ± 58.7 neurons) than in the VTA of eYFP mice (109.3 ± 11.2 neurons; Figures 4A–4D). By phenotyping VTA c-Fos-positive neurons, we found 10 times less c-Fos-VGaT neurons (16.67 ± 6.89 neurons; Figures 4E–4G) than c-Fos-VGluT2 neurons (169.33 ± 13.38 neurons) and determined that these c-Fos-VGluT2 neurons were more abundant in rostro-linear, parabrachial pigmented and rostral VTA nuclei (Table S2). These c-Fos findings further indicate that inputs from LHA-VGluT2 neurons to VTA preferentially activate VGluT2 neurons.

Given that previous viral-based mapping studies have shown that LH provides a major monosynaptic input to VTA-TH neurons (Watabe-Uchida et al., 2012), we examined the connectivity ratio by VTA photostimulation of LHA-VGluT2 fibers on VGluT2 and TH neurons by slice electrophysiology. We used TH::Cre transgenic mice for recordings of VTA-TH neurons after confirming selective expression of TH mRNA in transfected neurons (Figure S7). After VTA photostimulation, we found a higher proportion of VGluT2 responsive neurons than TH responsive neurons (Figures 4H–4K). These electrophysiological findings, together with the synaptic ultrastructural observations, indicate a preferential synaptic connectivity between LHA-VGluT2 and VTA-VGluT2 neurons.

VTA Photostimulation or Photoinhibition of LHA-VGluT2 Fibers Modulates Innate Escape Responses

To test the participation of LHA-VGluT2 fibers projecting to VTA in response to a looming stimulus, we tested mice that, in LHA-VGluT2 neurons, expressed ChR2-eYFP (ChR2-eYFP mice), eYFP (control mice), or halorhodopsin (Halo-eYFP mice; Figure S6). In the absence of VTA laser stimulation, we detected in all tested mice similar increases in the number of runs (Figure 5A) and speed (Figure S8; Table S3) in response to a looming stimulus, without changes in movement direction. In contrast, we found that VTA photostimulation of LHA-VGluT2 fibers increased the number of runs and speed in ChR2-eYFP, but not in eYFP mice (Figures 5A and S8). Conversely, VTA photoinhibition of LHA-VGluT2 fibers blocked looming-induced runs and speed (Figures 5A and S8).

We next examined the possible contribution of LHA-VGluT2 inputs to VTA in innate hiding responses, given that a recent study has proposed a role for VTA-GABA neurons in mediating flight-to-nest responses (Zhou et al., 2019). We tested responses

Figure 3. Within the VTA, LHA-VGluT2 Neurons Preferentially Establish Excitatory Synapses on VGluT2 Neurons

(A) Viral injection of AAV1-DIO-ChR2-mCherry into LHA and AAV1-DIO-eYFP into VTA of VGluT2::Cre mice.

(B) Confocal microscopy of VTA at low magnification; TH (blue), VGluT2-eYFP neurons (green), and VGluT2-mCherry fibers from LHA (red).

(C) Box in (B) at higher magnification showing TH neurons, VGluT2 neurons, and terminals (arrows and arrowheads) from LHA-VGluT2 neurons co-expressing mCherry and VGluT2 protein (white). Note terminals contacting soma (magenta arrow in neuron no. 1) and dendrites (magenta arrowheads) from VTA-VGluT2 neurons or contacting soma from a VTA-VGluT2-TH neuron (yellow arrow in neuron no. 2).

(D) Single VTA-VGluT2 dendrite (green outline with GFP detected by gold particles, arrowhead) making asymmetric synapses (green arrows) with three axon terminals ($AT_{1–3}$, red outlines) from LHA-VGluT2 neurons co-expressing mCherry (scattered dark material) and VGluT2 (arrowhead, gold particles). A VGluT2-negative dendrite (blue outline) makes an asymmetric synapse (green arrow) with a terminal (AT_4) from a LHA-VGluT2 neuron.

(E) Corresponding diagram.

(F) AT_3 at higher magnification.

(G) A VTA-VGluT2 soma (green outline with GFP detected by gold particles, arrowhead) making asymmetric synapses (green arrows) with two AT ($AT_{1–2}$, red outlines) from LHA-VGluT2 neurons co-expressing mCherry (scattered dark material) and VGluT2 (gold particles).

(H) Corresponding diagram.

(I) AT_1 at higher magnification.

(J) AT_2 at higher magnification.

(K) Within the VTA, LHA-VGluT2 axon terminals more frequently synapse on $VGluT2^+$ dendrites (699/1,420 LHA-VGluT2 terminals) than on TH^+ dendrites (538/1,690 LHA-VGluT2 terminals; $t_{(4)} = 2.81$, *p < 0.05, t test; data represent mean ± SEM).

(L) Evoked excitatory postsynaptic currents (EPSCs) at −60 mV (baseline, green trace) abolished by 10 μM CNQX (gray trace), but not by 10 μM bicuculline (pink trace).

(M) EPSCs amplitude in VTA-VGluT2 neurons (baseline: −39.08 ± 5.77 pA, bicuculline: −43.09 ± 6.71 pA, bicuculline + CNQX: −2.3 ± 0.32 pA; n = 11 neurons from 7 mice; $F_{(2,32)} = 35.97$, p < 0.001; ***p < 0.001 versus baseline, ANOVA with Dunnett's post hoc test; data represent mean ± SEM).

(N) EPSCs at −60 mV (baseline, green trace) abolished by 1 μM TTX (black trace) and restored by 200 μM 4AP (blue trace).

(O) EPSCs amplitude in VTA-VGluT2 neurons (baseline: −56.96 ± 9.13 pA, TTX: −10.04 ± 2.83 pA, TTX + 4AP: −74.85 ± 16.48 pA, CNQX: −9.72 ± 3.58 pA; n = 5 neurons from 3 mice; $F_{(3,19)} = 17.55$, p < 0.001; **p < 0.01 versus baseline, ANOVA with Dunnett's post hoc test; data represent mean ± SEM).

See also Figures S3–S5.

Please cite this article in press as: Barbano et al., VTA Glutamatergic Neurons Mediate Innate Defensive Behaviors, Neuron (2020), https://doi.org/10.1016/j.neuron.2020.04.024

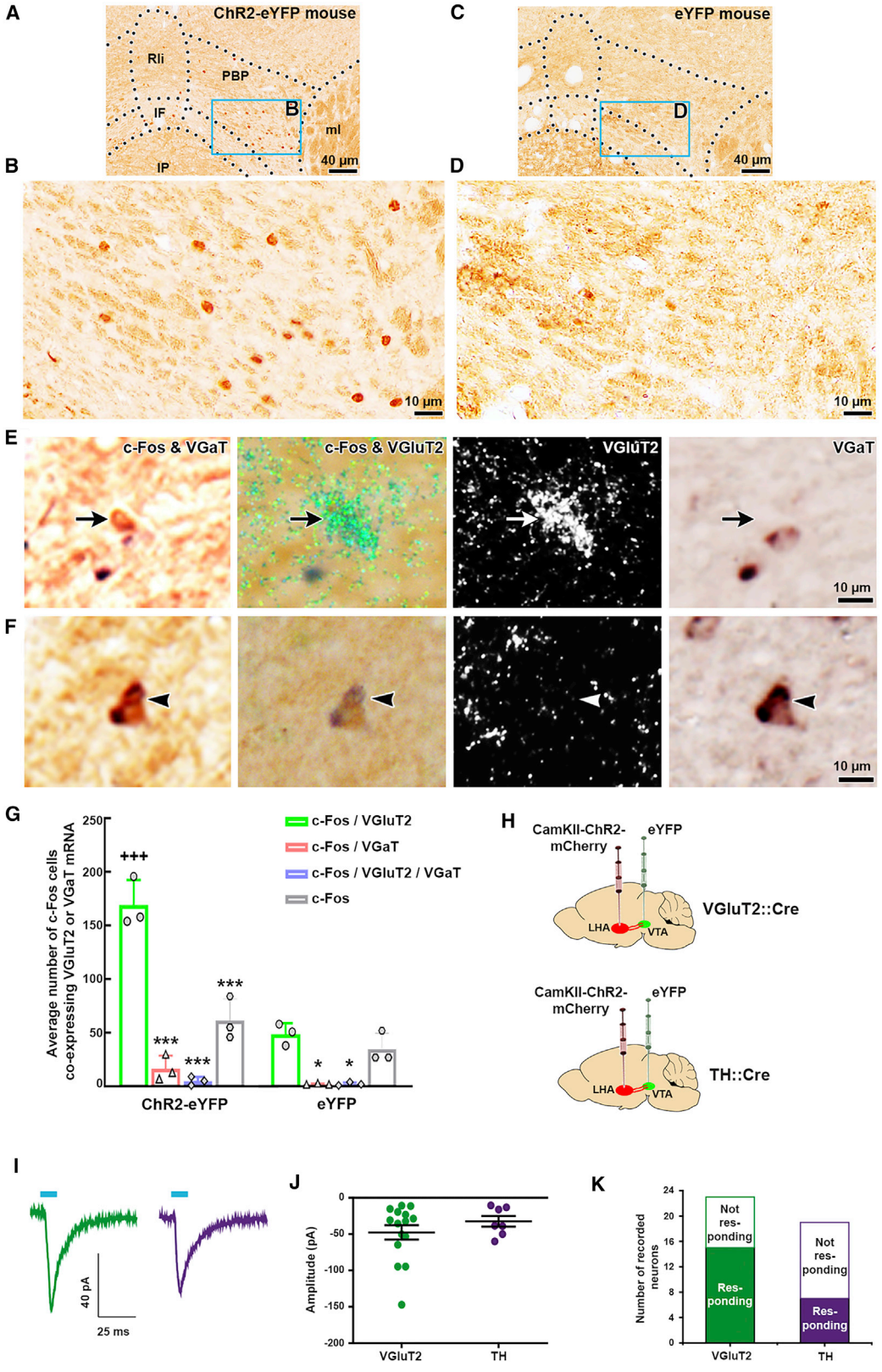

(legend on next page)

Please cite this article in press as: Barbano et al., VTA Glutamatergic Neurons Mediate Innate Defensive Behaviors, Neuron (2020), https://doi.org/10.1016/j.neuron.2020.04.024

to a looming stimulus under conditions in which a shelter was available for mice to hide and determined that, regardless of the presence or absence of a looming stimulus, mice spent long periods of time inside the shelter (Figure 5B). However, we found that VTA laser stimulation of LHA-VGluT2 fibers induced runs in ChR2-eYFP mice without affecting the number of runs in eYFP or Halo-eYFP mice (Figure 5B). We also found that VTA laser stimulation of LHA-VGluT2 fibers decreased the hiding time in ChR2-eYFP, but not in eYFP or Halo-eYFP mice (Figure S9A), indicating that activation of this pathway disrupted the shelter conferred safety. These findings indicate that LHA-VGluT2 inputs to VTA play a role in innate escape responses, but not in innate hiding responses.

We conducted a forced swim test to determine whether LHA-VGluT2 inputs to VTA play a role in escape responses during a threatening situation by placing mice in a container filled with water and measured mouse time duration of immobility through a laser-off epoch followed by a laser-on epoch. We found that all tested mice spent similar time immobile during the laser-off epoch (Figure S9B), but VTA laser stimulation of LHA-VGluT2 fibers during the laser-on epoch decreased time duration of immobility in ChR2-eYFP mice, increased time duration of immobility in Halo-eYFP mice, and maintained it in eYFP mice (Figure 5C). In addition, we observed that, toward the end of the laser-on epoch test, ChR2-eYFP mice kept swimming and Halo-eYFP mice had immobility duration higher than eYFP mice (Figure S9C). Consequently, we found that the total traveled distance and speed average were significantly higher in ChR2-eYFP mice than in eYFP mice (Figures S9D and S9E), but they shared similar maximum speed, indicating that both group of mice were capable of displaying swimming responses (Figure S9F).

Next, we tested whether VTA photostimulation of LHA-VGluT2 fibers induced anxiety in an open field test (Figure S9G). We found that VTA photostimulation of LHA-VGluT2 fibers did not alter the time that eYFP or ChR2-eYFP mice spent in the periphery or center zones (Figure S9H). These findings indicate that LHA-VGluT2 inputs to VTA play a role in escape responses during a threatening situation but do not mediate anxiety.

We also measured the latency for a mouse to escape a chamber where lemon or TMT odors were presented during VTA photostimulation or photoinhibition of LHA-VGluT2 fibers. We found that VTA photostimulation in ChR2-eYFP mice, but not in eYFP mice, induced escape from the lemon odor (Figure 5D). In contrast, we found a longer escape latency to TMT odor during VTA photoinhibition in Halo-eYFP mice (Figure 5D). These findings indicate that LHA-VGluT2 inputs to VTA play a role in escape behavior.

LHA-VGluT2 Neurons Projecting to VTA Are Activated by Innate Threats

We next injected a retrograde Cre-dependent GCaMP6s-expressing herpes simplex virus in VTA of VGluT2::Cre mice to measure Ca^{2+} activity in LHA-VGluT2 neurons innervating VTA (Figures 6A–6C). By *in vivo* fiber photometry, we detected increases in Ca^{2+} activity in LHA-VGluT2 neurons in response to looming stimulus (Figures 6D–6F) and in response to lemon or TMT odor exposure (Figures 6G–6I), but Ca^{2+} activity was higher in response to TMT (Figure 6I). These findings suggest that inputs from LHA-VGluT2 neurons synapsing on VTA are tuned to threatening stimuli.

Next, we determined the functional connectivity between LHA-VGluT2 neurons and VTA-VGluT2 neurons in mediating innate escape behavior by combining optogenetic and chemogenetic approaches. We tested mice expressing ChR2-eYFP or eYFP in LHA-VGluT2 neurons and expressing hM4D in VTA-VGluT2 neurons (Figures S10A–S10C). We confirmed that ChR2-eYFP mice, but not eYFP mice, presented with the neutral lemon odor behave as if it was a threatening predator odor during VTA laser stimulation of LHA-VGluT2 fibers (Figure 5D; Figure S10D); and we determined that the latency to escape was increased when VTA-VGluT2 neurons were inhibited by CNO injection in ChR2-eYFP mice (Figures S10D and S10E). These findings further support a role of LHA-VGluT2 neurons projecting to VTA-VGluT2 neurons in signaling threatening stimuli that induce innate escape responses.

DISCUSSION

Defensive behaviors are stereotyped actions that are naturally selected to increase the chances of survival across animal species. Although fighting and freezing have been widely studied, the

Figure 4. VTA Photostimulation of LHA-VGluT2 Fibers Induces c-Fos Expression Mostly in VGluT2 Neurons

(A and C) c-Fos expression (brown nuclei) induced by VTA photostimulation of LHA-VGluT2 fibers in ChR2-eYFP (A) or eYFP mice (C).

(B) Box in (A) at higher magnification.

(D) Box in (C) at higher magnification.

(E) Neuron co-expressing c-Fos and VGluT2, lacking VGaT mRNA (arrow).

(F) Neuron co-expressing c-Fos and VGaT mRNA, lacking VGluT2 mRNA (arrowhead).

(G) VTA number of c-Fos neurons was higher in ChR2-eYFP mice (252.67 ± 17.33; n = 3, 9 sections/mouse) than in eYFP mice (89.00 ± 2.31; n = 3, 9 section/mouse; $t_{(4)} = 9.36$, $p < 0.001$, t test). Within VTA of ChR2-eYFP mice, most of c-Fos neurons co-expressed VGluT2 mRNA (169.33 ± 13.38; 508 neurons), fewer co-expressed VGaT (16.67 ± 6.89; 50 neurons) or VGluT2 and VGaT (5.00 ± 2.31; 7 neurons), and two thirds lacked both VGluT2 and VGaT mRNA (61.67 ± 11.46, 106 neurons; cell type: $F_{(3,6)} = 58.36$, $p < 0.001$, ANOVA with Newman-Keuls post hoc test; data represent mean ± SEM). Asterisks indicate significant differences against c-Fos/VGluT2 neuronal subtype. ***$p < 0.001$. Plus signs indicate differences against eYFP mice. +++ $p < 0.001$.

(H) Viral injection of AAV1-CamKII-ChR2-mCherry into LHA and AAV1-DIO-eYFP into VTA of VGluT2::Cre or TH::Cre mice.

(I–K) Recordings of VTA-VGluT2 (green) and VTA-TH (purple) neurons in response to VTA photostimulation.

(I) Voltage clamp trace of a VTA-VGluT2 neuron and a VTA-TH neuron after VTA photostimulation (blue rectangle).

(J) EPSCs amplitude in VGluT2 or TH neurons is not significantly different (t test, $t_{(20)} = 0.9915$, $p = 0.33$; data represent mean ± SEM).

(K) Number of photostimulation responding VTA-VGluT2 (15 out of 23; 4 mice) and VTA-TH (7 out of 19; 3 mice) neurons.

See also Figures S6 and S7 and Table S2.

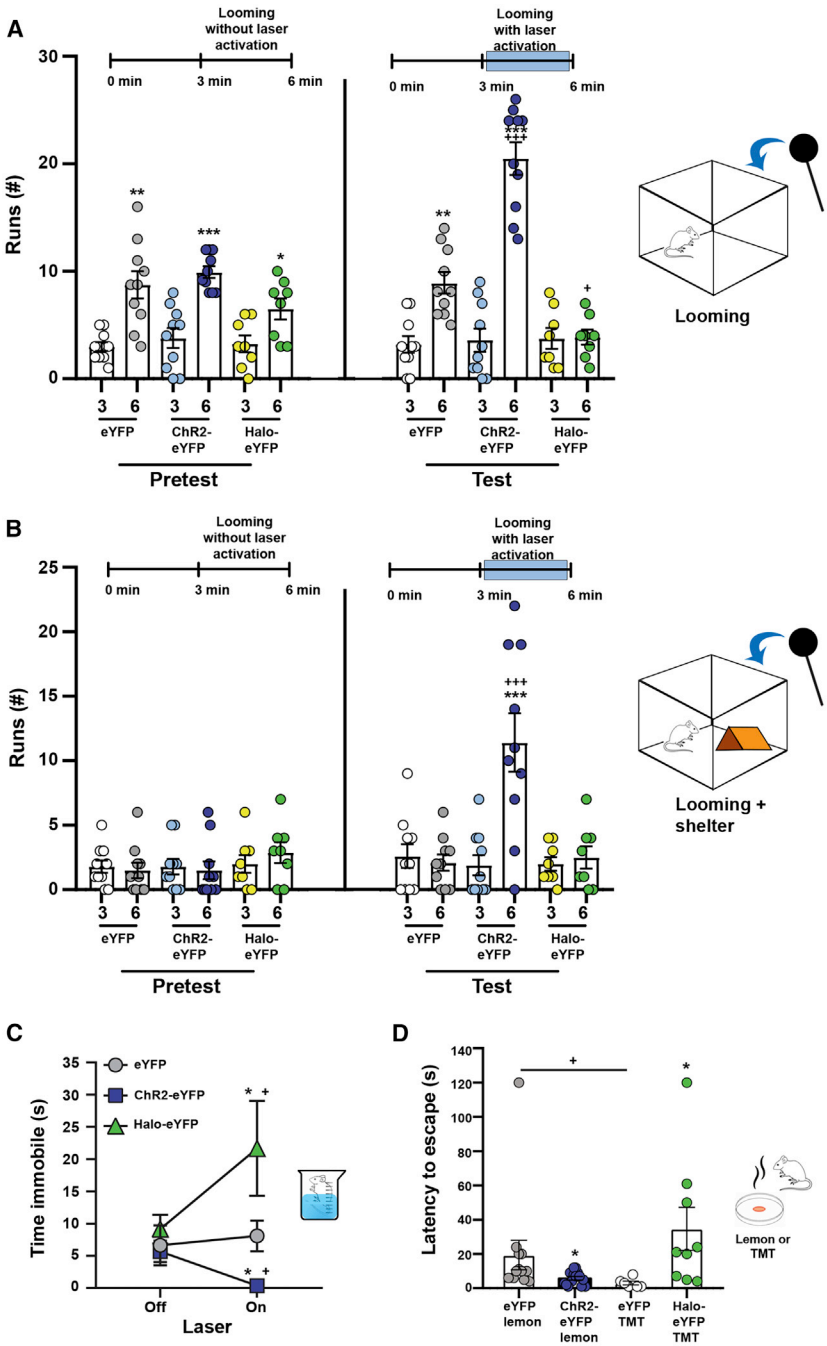

Figure 5. VTA Photostimulation or Photoinhibition of LHA-VGluT2 Fibers Modulates Innate Escape Responses

(A) Runs induced by a looming stimulus during VTA photostimulation or photoinhibition of LHA-VGluT2 fibers, in absence of shelter. Looming increases runs in all tested mouse groups (left), but laser activation further increased runs in ChR2-eYFP mice, and laser inactivation decreased runs in Halo-eYFP mice (right; eYFP, n = 10; ChR2-eYFP, n = 10; Halo-eYFP, n = 8; group × experimental phase × time: $F_{(2,25)} = 18.40$, $p < 0.001$, ANOVA with Newman-Keuls post hoc test; data represent mean ± SEM). *$p < 0.05$, **$p < 0.01$, and ***$p < 0.001$ against the first 3 min of the experiment, for each group; +$p < 0.05$ and +++$p < 0.001$ against the same period in the pretest phase.

(B) Runs induced by a looming stimulus during VTA photostimulation or photoinhibition of LHA-VGluT2 fibers in the presence of shelter. In the absence of laser activation, mice from all groups hided in the shelter and looming did not induce runs (left). Laser activation induced runs in ChR2-eYFP mice (right; eYFP, n = 10; ChR2-eYFP, n = 10; Halo-eYFP, n = 8; group × experimental phase × time: $F_{(2,25)} = 14.55$, $p < 0.001$, ANOVA with Newman-Keuls post hoc test; data represent mean ± SEM). ***$p < 0.001$ against the first 3 min of the experiment for each group; +++$p < 0.001$ against the same period in the pretest phase.

(C) Total time immobile during forced swim test before and during VTA photostimulation or photoinhibition of LHA-VGluT2 fibers (eYFP, n = 9; ChR2-eYFP, n = 9; Halo-eYFP, n = 11; group × experimental phase: $F_{(2,26)} = 4.25$, $p < 0.05$, ANOVA with Newman-Keuls post hoc test; data represent mean ± SEM). *$p < 0.05$ against eYFP; +$p < 0.05$ against laser off.

(D) Escape latency from lemon or TMT odor (eYFP lemon, n = 13; ChR2-eYFP lemon, n = 14; eYFP TMT, n = 6; Halo-eYFP TMT, n = 9; group: $F_{(3,38)} = 3.17$, $p = 0.05$, ANOVA with Newman-Keuls post hoc test; data represent mean ± SEM). *$p < 0.05$ against corresponding eYFP group; +$p < 0.05$ between eYFP groups.

See also Figures S6, S8, and S9 and Table S3.

neurocircuitry underlying innate escape responses, crucial components of the defensive repertoire, remains unclear. Whereas previous studies have suggested that different types of VTA neurons (dopamine, GABA, and glutamate) encode responses to aversive or appetitive stimuli (Brischoux et al., 2009; Bromberg-Martin et al., 2010; Lammel et al., 2014; Tan et al., 2012; de Jong et al., 2019; Nieh et al., 2016; Wang et al., 2015b; Root et al., 2014b, 2018; Qi et al., 2016), we now demonstrated an unanticipated role of VTA-glutamate neurons in signaling the presence of both a predator odor and the attack of a predator. In addition, we demonstrated that VTA-glutamate neurons play a role in innate escape responses by showing that either genetic ablation or chemogenetic inhibition of VTA-glutamate neurons is sufficient to disrupt innate escape responses. Moreover, we demonstrated that VTA-glutamate neurons receive a major excitatory input from LHA-glutamate neurons, input that, by releasing glutamate in VTA, induces innate escape responses, but not innate hiding responses. Although prior studies have shown that LH-GABA (Barbano et al., 2016; Nieh et al., 2015) and LH-glutamate (de Jong et al., 2019; Nieh et al., 2016) inputs to VTA play a role in different aspects of motivated behavior, we demonstrated here that a specific role for VTA-projecting subset of LHA-glutamate neurons is to support innate defensive behavior.

We detected increases in VTA-glutamate neuronal activity in response to innate threatening stimuli (a predator odor or attack of a predator) and found that escape responses to these stimuli

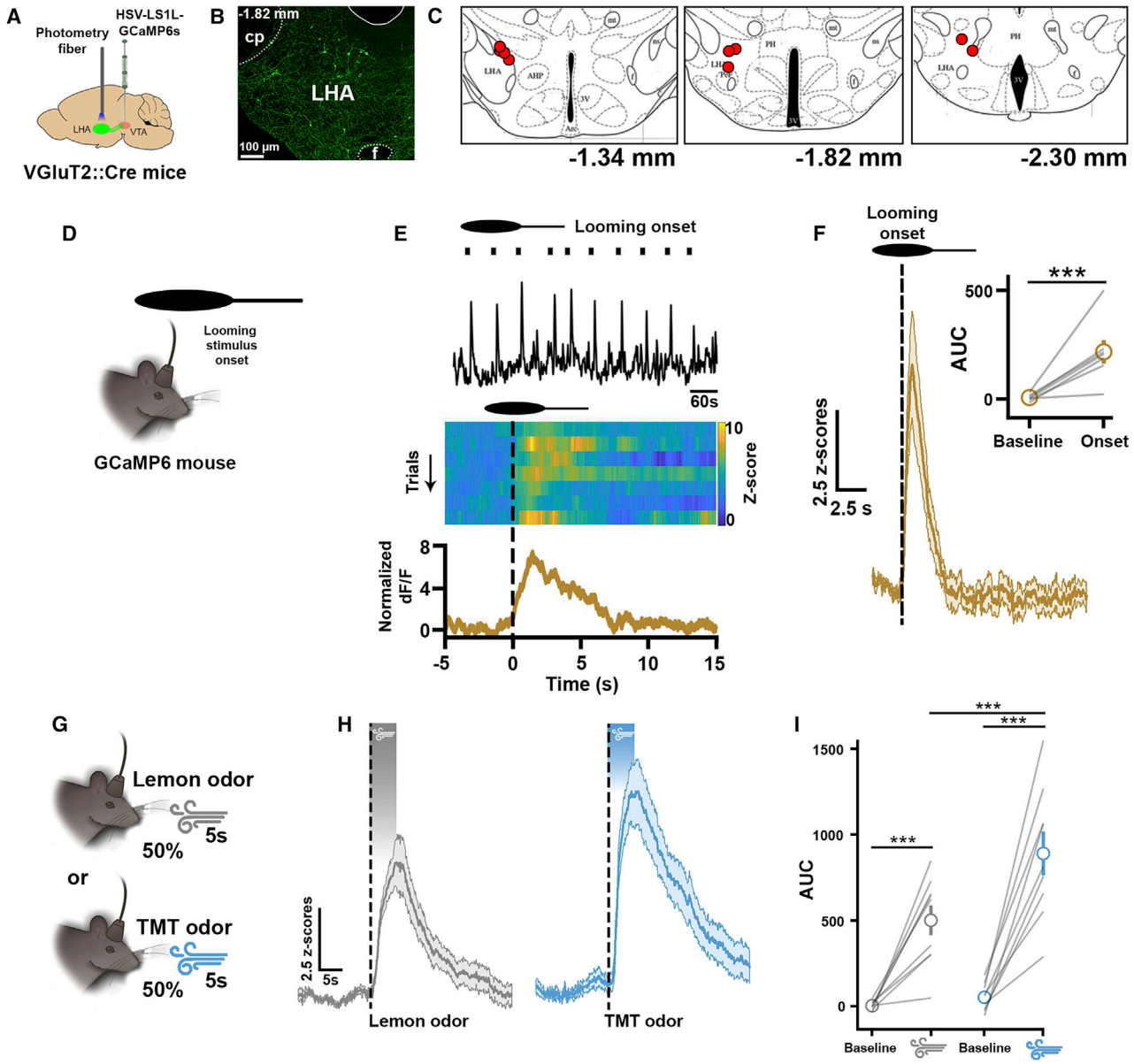

Figure 6. LHA-VGluT2 Neurons Projecting to VTA Are Activated by Innate Threats

(A) VTA injection of retrograde virus HSV-LS1L-GCaMP6s and LHA photometry fiber.

(B) VTA retrograde LHA-VGluT2 neurons expressing GCamP6s-GFP below photometry fiber.

(C) LHA photometry fiber placements.

(D) Schematic representation of the looming stimulus.

(E) Whole session recording of LHA-VGluT2 neurons projecting to VTA showing time of looming stimulus onset (top), heatmap of Ca^{2+} activity over successive looming trials (middle), and cell population responses to looming stimulus onset showing increases in Ca^{2+} activity in LHA-VGluT2 neurons projecting to VTA (bottom).

(F) Population Ca^{2+} activity (+SEM) in LHA-VGluT2 neurons, projecting to VTA, during looming stimulus onset. Inset: AUC for Ca^{2+} activity in LHA-VGluT2 neurons, projecting to VTA, before (−5 to 0 s, baseline) and after (0–5 s, onset) onset of the looming stimulus is shown (n = 7; t test; $t_{(112)} = 10.94$, ***$p < 0.001$; data represent mean ± SEM).

(G) Schematic representation of odor test.

(H) Population Ca^{2+} activity (+SEM) in LHA-VGluT2 neurons, projecting to VTA, in response to lemon (left) or TMT (right) odor.

(I) AUC for Ca^{2+} activity in LHA-VGluT2 neurons, projecting to VTA, in response to lemon or TMT odor (n = 9; odor × epoch: $F_{(1,342)} = 17.25$, $p < 0.001$, ANOVA with Bonferroni post hoc test; ***$p < 0.001$; data represent mean ± SEM).

See also Figure S10.

Please cite this article in press as: Barbano et al., VTA Glutamatergic Neurons Mediate Innate Defensive Behaviors, Neuron (2020), https://doi.org/10.1016/j.neuron.2020.04.024

are decreased by the genetic ablation or chemogenetic inhibition of VTA-glutamate neurons. Based on these findings, we conclude that VTA-glutamate neurons play a role in encoding innate defensive escape responses. In contrast, we found that genetic ablation of VTA-GABA neurons did not modify the innate escape responses to predator odor or a looming stimulus. However, a recent study has shown that VTA-GABA neurons play a role in looming-evoked flight-to-nest behavior, regulated by glutamatergic inputs from the superior colliculus to VTA-GABA neurons (Zhou et al., 2019). Thus, it seems that VTA-GABA neurons mediate safety by promoting hiding behavior, although VTA-glutamate neurons mediate safety by promoting escape. These findings on VTA-glutamate and VTA-GABA neurons together with recent studies showing that VTA-dopamine neurons are activated by predator odor (Moriya et al., 2018) indicate that diverse types of VTA neurons participate in different aspects of innate fear responses.

We provide synaptic ultrastructural evidence demonstrating that axon terminals from LHA-glutamate neurons establish multiple asymmetric synapses on both cell bodies and dendrites of VTA-glutamate neurons and, by electrophysiological analysis, determined that VTA-glutamate neurons fire in response to monosynaptic release of glutamate from presynaptic LHA-glutamate inputs. Given that LHA-glutamate projections provide multiple synaptic sites for the release of glutamate along the cell bodies and dendrites of VTA-glutamate neurons, it is likely that, during *in vivo* conditions, the LHA-glutamate neurons exert a stronger excitatory regulation on VTA-VGluT2 neurons than on VTA-dopamine neurons, where the number of synaptic sites by LHA-glutamate neurons is lower and restricted to dendrites.

LH excitatory projections promote active avoidance, aversion, and escape from a looming stimulus by releasing glutamate in the lateral habenula (Lecca et al., 2017; Stamatakis et al., 2016) or the VTA (de Jong et al., 2019; Nieh et al., 2016) and promote escape responses by releasing glutamate in the periaqueductal gray (Li et al., 2018). We now present converging evidence indicating that LHA provides a major glutamate input to VTA-glutamate neurons and that VTA activation of LHA-glutamate inputs promotes escape responses in mice facing threatening situations. In contrast, VTA photoinhibition of LHA-glutamate inputs decreases escape responses in mice confronted with forced swimming, predator odor, or a looming stimulus mimicking an approaching aerial predator. Furthermore, by Ca^{2+} recording, we demonstrated that LHA-glutamate neurons that project to VTA signal threatening stimuli.

Recent circuit-based behavioral studies have established the role of LH glutamatergic inputs to VTA in place avoidance and aversion (de Jong et al., 2019; Nieh et al., 2016). Findings from this previous work have shown that inputs from LH-glutamate neurons synapsing on VTA-GABA neurons mediate place avoidance (Nieh et al., 2016). Given that, in this study, place avoidance was accompanied by a decrease in dopamine release within the nAcc, it has been concluded that place avoidance is mediated by LH-glutamate neurons synapsing on VTA-GABA interneurons and proposed that GABA release from these interneurons resulted in the inhibition of VTA-dopamine neurons innervating the nAcc (Nieh et al., 2016). Although we did not investigate the role in aversion by LHA-glutamate inputs on VTA-GABA neurons, we found that optogenetic VTA stimulation of LHA-glutamate fibers results in c-Fos expression in ten VTA-glutamate neurons for each VTA-GABA neuron. Thus, the reported nAcc decrease in dopamine following VTA photoactivation of LHA-glutamate inputs may involve a selective subset of VTA-GABA neurons synapsing on mesoaccumbens dopamine neurons. In support to the heterogeneity among VTA-GABA neurons, the VTA-GABA neurons that participate in looming-evoked flight-to-nest behavior receive glutamatergic inputs from superior colliculus and project to the central amygdala (Zhou et al., 2019). Regarding VTA-dopamine neurons, a recent study has shown that both unexpected aversive outcomes and cues that predict them induced dopamine release and calcium responses in the ventromedial nAcc shell (de Jong et al., 2019). Moreover, it has been proposed that the increase of dopamine is mediated by LH-glutamate inputs synapsing on VTA-dopamine neurons that project to ventral nAcc medial shell (de Jong et al., 2019). These previous findings suggesting monosynaptic excitatory synapses between glutamatergic inputs from LH and both VTA-GABA (Nieh et al., 2016) and VTA-dopamine (de Jong et al., 2019) neurons, together with the demonstration that LHA-glutamate neurons establish multiple excitatory synapses on VTA-glutamate neurons, underlie the complexity of the neuronal circuitry between the LHA-glutamate neurons and the diverse phenotypes of postsynaptic VTA neurons. In addition to the involvement of LHA-glutamatergic inputs to VTA in escape behavior, LH-glutamatergic inputs to the lateral habenula or the periaqueductal gray have been involved in innate escape behavior (Lecca et al., 2017; Li et al., 2018), highlighting the crucial role of LHA-glutamate neurons in defensive responses. Given that escaping from imminent danger is critical for survival and requires the integration of complex information from the environment, a complex neuronal circuitry is expected to mediate specific aspects of escape behavior.

Although here we demonstrate a role of VTA-VGluT2 neurons in innate defensive behavior, we have earlier shown that a subset of VTA-VGluT2 neurons participate in aversion, place avoidance, or place preference (Dobi et al., 2010; Wang et al., 2015b; Root et al., 2014b; Qi et al., 2016). By single-cell recordings, we have previously demonstrated that VTA-VGluT2 neurons increase their neuronal activity in response to an aversive stimulus, but subpopulations of VTA-VGluT2 neurons are differentially affected by sucrose reward (Root et al., 2018). Here, by calcium imaging, we detected increases of VTA-VGluT2 neuronal activity in response to an aversive stimulus (tail lift). In contrast, we did not detect significant changes in calcium activity by rewarding food, which may be explained by the lack of resolution in bulk calcium recording. At the level of circuitry, we have demonstrated that VTA-VGluT2 neurons play a role in place preference by establishing monosynaptic excitatory synapses on neighboring mesoaccumbens dopamine neurons (Dobi et al., 2010; Wang et al., 2015b). In contrast, we found that VTA-VGluT2 neurons mediate place avoidance by targeting glutamatergic neurons in the lateral habenula (Root et al., 2014b) or parvalbumin GABA interneurons in nAcc (Qi et al., 2016). Although it remains to be determined the source of inputs to the subset of VTA-VGluT2 neurons mediating reward or aversion, studies by the group of Tye have shown that glutamate release from LH inputs into VTA drives aversion (Nieh et al., 2016). Within this context,

future studies are necessary to determine the extent to which different or overlapping subtypes of LHA-glutamate neurons regulate VTA-VGluT2 neurons participating in aversion or innate defensive behavior.

In conclusion, we uncovered a role for VTA-glutamate neurons in the modulation of innate defensive behaviors and propose that relevant information on how to cope with threatening situations is conveyed to VTA-glutamate neurons by LHA-glutamate neurons. These findings may be relevant for neuropsychiatric disorders, such as autism spectrum disorder (ASD), where inability to differentiate threat from safe cues has been demonstrated (Top et al., 2016). Additionally, patients suffering from ASD show impairment in detecting social chemosignals, like the smell of fear (Endevelt-Shapira et al., 2018). Given that VTA-glutamate neurons have been implicated in sociability deficits associated with alterations in the ASD-related gene, Ube3a (Krishnan et al., 2017), we speculate that VTA-glutamate neurons may be part of a circuitry encoding innate defensive behaviors that, when dysregulated, may lead to disease states.

STAR★METHODS

Detailed methods are provided in the online version of this paper and include the following:

- KEY RESOURCES TABLE
- RESOURCE AVAILABILITY
  - Lead contact
  - Materials availability
  - Data and code availability
- EXPERIMENTAL MODEL AND SUBJECT DETAILS
- METHOD DETAILS
  - Surgeries for anatomical studies
  - Surgeries for EM or electrophysiology
  - Surgeries for behavioral studies
  - Histological verification
  - In situ hybridization (ISH)
  - Electron and confocal microscopy
  - Electrophysiology
  - Fiber photometry
  - Behavioral studies
- QUANTIFICATION AND STATISTICAL ANALYSIS

SUPPLEMENTAL INFORMATION

Supplemental Information can be found online at https://doi.org/10.1016/j.neuron.2020.04.024.

ACKNOWLEDGMENTS

This work was supported by the Intramural Research Program (IRP) of the National Institute on Drug Abuse (IRP/NIDA/NIH) and a NIDA K99/R00 pathway to independence award (DA043572; to D.J.B.). We thank the NIDA/IRP Genetic Engineering and Viral Vector Core for manufactured viral vectors. The pAAV-Flex-taCasp3-TEVp was a gift from Nirao Shah and Jim Wells. We thank Rong Ye and Kevin Yu from the NIDA/IRP Confocal and Electron Microscopy Core for collecting confocal and immuno-electron microscopic images, Marc Raley from Visual Media Services for graphic design assistance, and Carlos Mejias-Aponte for suggestions on chemogenetic studies.

AUTHOR CONTRIBUTIONS

M.M. and M.F.B. conceptualized the project. M.F.B. and H.-L.W. performed behavioral studies. M.F.B. performed pharmacological studies and data analysis. M.F.B., H.-L.W., and B.L. performed neuroanatomical studies. S.Z. performed anatomical and ultrastructural studies and data analysis. J.M.-B. performed *ex vivo* recordings and data analysis. M.F.B., D.J.E., and D.J.B. performed photometry and data analysis. H.-L.W. and A.F.-G. quantified neuronal phenotypes. M.M. and M.F.B. prepared the manuscript with contribution from all co-authors.

DECLARATION OF INTERESTS

The authors declare no competing interests.

Received: November 21, 2019
Revised: April 7, 2020
Accepted: April 27, 2020
Published: May 21, 2020

REFERENCES

Barbano, M.F., Wang, H.-L., Morales, M., and Wise, R.A. (2016). Feeding and reward are differentially induced by activating GABAergic lateral hypothalamic projections to VTA. J. Neurosci. *36*, 2975–2985.

Beier, K.T., Gao, X.J., Xie, S., DeLoach, K.E., Malenka, R.C., and Luo, L. (2019). Topological organization of ventral tegmental area connectivity revealed by viral-genetic dissection of input-output relations. Cell Rep. *26*, 159–167.e6.

Berridge, K.C., and Robinson, T.E. (1998). What is the role of dopamine in reward: hedonic impact, reward learning, or incentive salience? Brain Res. Brain Res. Rev. *28*, 309–369.

Berrios, J., Stamatakis, A.M., Kantak, P.A., McElligott, Z.A., Judson, M.C., Aita, M., Rougie, M., Stuber, G.D., and Philpot, B.D. (2016). Loss of UBE3A from TH-expressing neurons suppresses GABA co-release and enhances VTA-NAc optical self-stimulation. Nat. Commun. *7*, 10702.

Brischoux, F., Chakraborty, S., Brierley, D.I., and Ungless, M.A. (2009). Phasic excitation of dopamine neurons in ventral VTA by noxious stimuli. Proc. Natl. Acad. Sci. USA *106*, 4894–4899.

Bromberg-Martin, E.S., Matsumoto, M., and Hikosaka, O. (2010). Dopamine in motivational control: rewarding, aversive, and alerting. Neuron *68*, 815–834.

Chen, T.W., Wardill, T.J., Sun, Y., Pulver, S.R., Renninger, S.L., Baohan, A., Schreiter, E.R., Kerr, R.A., Orger, M.B., Jayaraman, V., et al. (2013). Ultrasensitive fluorescent proteins for imaging neuronal activity. Nature *499*, 295–300.

De Franceschi, G., Vivattanasarn, T., Saleem, A.B., and Solomon, S.G. (2016). Vision guides selection of freeze or flight defense strategies in mice. Curr. Biol. *26*, 2150–2154.

de Jong, J.W., Afjei, S.A., Pollak Dorocic, I., Peck, J.R., Liu, C., Kim, C.K., Tian, L., Deisseroth, K., and Lammel, S. (2019). A neural circuit mechanism for encoding aversive stimuli in the mesolimbic dopamine system. Neuron *101*, 133–151.e7.

Deng, H., Xiao, X., and Wang, Z. (2016). Periaqueductal gray neuronal activities underlie different aspects of defensive behaviors. J. Neurosci. *36*, 7580–7588.

Dobi, A., Margolis, E.B., Wang, H.-L., Harvey, B.K., and Morales, M. (2010). Glutamatergic and nonglutamatergic neurons of the ventral tegmental area establish local synaptic contacts with dopaminergic and nondopaminergic neurons. J. Neurosci. *30*, 218–229.

Eilam, D. (2005). Die hard: a blend of freezing and fleeing as a dynamic defense–implications for the control of defensive behavior. Neurosci. Biobehav. Rev. *29*, 1181–1191.

Endevelt-Shapira, Y., Perl, O., Ravia, A., Amir, D., Eisen, A., Bezalel, V., Rozenkrantz, L., Mishor, E., Pinchover, L., Soroka, T., et al. (2018). Altered

responses to social chemosignals in autism spectrum disorder. Nat. Neurosci. *21*, 111–119.

Evans, D.A., Stempel, A.V., Vale, R., Ruehle, S., Lefler, Y., and Branco, T. (2018). A synaptic threshold mechanism for computing escape decisions. Nature *558*, 590–594.

Faget, L., Osakada, F., Duan, J., Ressler, R., Johnson, A.B., Proudfoot, J.A., Yoo, J.H., Callaway, E.M., and Hnasko, T.S. (2016). Afferent inputs to neurotransmitter-defined cell types in the ventral tegmental area. Cell Rep. *15*, 2796–2808.

Fiorillo, C.D., Song, M.R., and Yun, S.R. (2013). Multiphasic temporal dynamics in responses of midbrain dopamine neurons to appetitive and aversive stimuli. J. Neurosci. *33*, 4710–4725.

Geisler, S., Derst, C., Veh, R.W., and Zahm, D.S. (2007). Glutamatergic afferents of the ventral tegmental area in the rat. J. Neurosci. *27*, 5730–5743.

Gradinaru, V., Zhang, F., Ramakrishnan, C., Mattis, J., Prakash, R., Diester, I., Goshen, I., Thompson, K.R., and Deisseroth, K. (2010). Molecular and cellular approaches for diversifying and extending optogenetics. Cell *141*, 154–165.

Gross, C.T., and Canteras, N.S. (2012). The many paths to fear. Nat. Rev. Neurosci. *13*, 651–658.

Huang, L., Yuan, T., Tan, M., Xi, Y., Hu, Y., Tao, Q., Zhao, Z., Zheng, J., Han, Y., Xu, F., et al. (2017). A retinoraphe projection regulates serotonergic activity and looming-evoked defensive behaviour. Nat. Commun. *8*, 14908.

Krashes, M.J., Koda, S., Ye, C., Rogan, S.C., Adams, A.C., Cusher, D.S., Maratos-Flier, E., Roth, B.L., and Lowell, B.B. (2011). Rapid, reversible activation of AgRP neurons drives feeding behavior in mice. J. Clin. Invest. *121*, 1424–1428.

Krishnan, V., Stoppel, D.C., Nong, Y., Johnson, M.A., Nadler, M.J., Ozkaynak, E., Teng, B.L., Nagakura, I., Mohammad, F., Silva, M.A., et al. (2017). Autism gene Ube3a and seizures impair sociability by repressing VTA Cbln1. Nature *543*, 507–512.

Lammel, S., Lim, B.K., and Malenka, R.C. (2014). Reward and aversion in a heterogeneous midbrain dopamine system. Neuropharmacology *76* (Pt B), 351–359.

Lecca, S., Meye, F.J., Trusel, M., Tchenio, A., Harris, J., Schwarz, M.K., Burdakov, D., Georges, F., and Mameli, M. (2017). Aversive stimuli drive hypothalamus-to-habenula excitation to promote escape behavior. eLife *6*, e30697.

LeDoux, J., and Daw, N.D. (2018). Surviving threats: neural circuit and computational implications of a new taxonomy of defensive behaviour. Nat. Rev. Neurosci. *19*, 269–282.

Lerner, T.N., Shilyansky, C., Davidson, T.J., Evans, K.E., Beier, K.T., Zalocusky, K.A., Crow, A.K., Malenka, R.C., Luo, L., Tomer, R., and Deisseroth, K. (2015). Intact-brain analyses reveal distinct information carried by SNc dopamine subcircuits. Cell *162*, 635–647.

Li, Y., Zeng, J., Zhang, J., Yue, C., Zhong, W., Liu, Z., Feng, Q., and Luo, M. (2018). Hypothalamic circuits for predation and evasion. Neuron *97*, 911–924.e5.

Matsumoto, H., Tian, J., Uchida, N., and Watabe-Uchida, M. (2016). Midbrain dopamine neurons signal aversion in a reward-context-dependent manner. eLife *5*, e17328.

Mongeau, R., Miller, G.A., Chiang, E., and Anderson, D.J. (2003). Neural correlates of competing fear behaviors evoked by an innately aversive stimulus. J. Neurosci. *23*, 3855–3868.

Morales, M., and Margolis, E.B. (2017). Ventral tegmental area: cellular heterogeneity, connectivity and behaviour. Nat. Rev. Neurosci. *18*, 73–85.

Moriya, S., Yamashita, A., Kawashima, S., Nishi, R., Yamanaka, A., and Kuwaki, T. (2018). Acute aversive stimuli rapidly increase the activity of ventral tegmental area dopamine neurons in awake mice. Neuroscience *386*, 16–23.

Nieh, E.H., Matthews, G.A., Allsop, S.A., Presbrey, K.N., Leppla, C.A., Wichmann, R., Neve, R., Wildes, C.P., and Tye, K.M. (2015). Decoding neural circuits that control compulsive sucrose seeking. Cell *160*, 528–541.

Nieh, E.H., Vander Weele, C.M., Matthews, G.A., Presbrey, K.N., Wichmann, R., Leppla, C.A., Izadmehr, E.M., and Tye, K.M. (2016). Inhibitory input from the lateral hypothalamus to the ventral tegmental area disinhibits dopamine neurons and promotes behavioral activation. Neuron *90*, 1286–1298.

Osakada, F., Mori, T., Cetin, A.H., Marshel, J.H., Virgen, B., and Callaway, E.M. (2011). New rabies virus variants for monitoring and manipulating activity and gene expression in defined neural circuits. Neuron *71*, 617–631.

Paxinos, G., and Franklin, K.B.J. (2001). The Mouse Brain in Stereotaxic Coordinates (Academic).

Peters, A., Palay, S.L., and Webster, H.D. (1991). The Fine Structure of the Nervous System: Neurons and Their Supporting Cells (Oxford University).

Qi, J., Zhang, S., Wang, H.L., Wang, H., de Jesus Aceves Buendia, J., Hoffman, A.F., Lupica, C.R., Seal, R.P., and Morales, M. (2014). A glutamatergic reward input from the dorsal raphe to ventral tegmental area dopamine neurons. Nat. Commun. *5*, 5390.

Qi, J., Zhang, S., Wang, H.L., Barker, D.J., Miranda-Barrientos, J., and Morales, M. (2016). VTA glutamatergic inputs to nucleus accumbens drive aversion by acting on GABAergic interneurons. Nat. Neurosci. *19*, 725–733.

Richie, C.T., Whitaker, L.R., Whitaker, K.W., Necarsulmer, J., Baldwin, H.A., Zhang, Y., Fortuno, L., Hinkle, J.J., Koivula, P., Henderson, M.J., et al. (2017). Near-infrared fluorescent protein iRFP713 as a reporter protein for optogenetic vectors, a transgenic Cre-reporter rat, and other neuronal studies. J. Neurosci. Methods *284*, 1–14.

Root, D.H., Mejias-Aponte, C.A., Zhang, S., Wang, H.L., Hoffman, A.F., Lupica, C.R., and Morales, M. (2014a). Single rodent mesohabenular axons release glutamate and GABA. Nat. Neurosci. *17*, 1543–1551.

Root, D.H., Mejias-Aponte, C.A., Qi, J., and Morales, M. (2014b). Role of glutamatergic projections from ventral tegmental area to lateral habenula in aversive conditioning. J. Neurosci. *34*, 13906–13910.

Root, D.H., Estrin, D.J., and Morales, M. (2018). Aversion or salience signaling by ventral tegmental area glutamate neurons. iScience *2*, 51–62.

Rosen, J.B., Asok, A., and Chakraborty, T. (2015). The smell of fear: innate threat of 2,5-dihydro-2,4,5-trimethylthiazoline, a single molecule component of a predator odor. Front. Neurosci. *9*, 292.

Schultz, W. (2016). Dopamine reward prediction-error signalling: a two-component response. Nat. Rev. Neurosci. *17*, 183–195.

Stamatakis, A.M., Van Swieten, M., Basiri, M.L., Blair, G.A., Kantak, P., and Stuber, G.D. (2016). Lateral hypothalamic area glutamatergic neurons and their projections to the lateral habenula regulate feeding and reward. J. Neurosci. *36*, 302–311.

Tan, K.R., Yvon, C., Turiault, M., Mirzabekov, J.J., Doehner, J., Labouèbe, G., Deisseroth, K., Tye, K.M., and Lüscher, C. (2012). GABA neurons of the VTA drive conditioned place aversion. Neuron *73*, 1173–1183.

Top, D.N., Jr., Stephenson, K.G., Doxey, C.R., Crowley, M.J., Kirwan, C.B., and South, M. (2016). Atypical amygdala response to fear conditioning in autism spectrum disorder. Biol. Psychiatry Cogn. Neurosci. Neuroimaging *1*, 308–315.

Wang, L., Chen, I.Z., and Lin, D. (2015a). Collateral pathways from the ventromedial hypothalamus mediate defensive behaviors. Neuron *85*, 1344–1358.

Wang, H.-L., Qi, J., Zhang, S., Wang, H., and Morales, M. (2015b). Rewarding effects of optical stimulation of ventral tegmental area glutamatergic neurons. J. Neurosci. *35*, 15948–15954.

Watabe-Uchida, M., Zhu, L., Ogawa, S.K., Vamanrao, A., and Uchida, N. (2012). Whole-brain mapping of direct inputs to midbrain dopamine neurons. Neuron *74*, 858–873.

Wei, P., Liu, N., Zhang, Z., Liu, X., Tang, Y., He, X., Wu, B., Zhou, Z., Liu, Y., Li, J., et al. (2015). Processing of visually evoked innate fear by a non-canonical thalamic pathway. Nat. Commun. *6*, 6756.

Wilson, W.J., and Hall, J.C. (1988). Lesions of the mesolimbic dopamine system disrupt signalled escape responses in the rat. Acta Neurobiol. Exp. (Warsz.) *48*, 117–121.

Wise, R.A. (2004). Dopamine, learning and motivation. Nat. Rev. Neurosci. *5*, 483–494.

Yamaguchi, T., Wang, H.L., Li, X., Ng, T.H., and Morales, M. (2011). Mesocorticolimbic glutamatergic pathway. J. Neurosci. *31*, 8476–8490.

Yang, C.F., Chiang, M.C., Gray, D.C., Prabhakaran, M., Alvarado, M., Juntti, S.A., Unger, E.K., Wells, J.A., and Shah, N.M. (2013). Sexually dimorphic neurons in the ventromedial hypothalamus govern mating in both sexes and aggression in males. Cell *153*, 896–909.

Zhang, S., Qi, J., Li, X., Wang, H.L., Britt, J.P., Hoffman, A.F., Bonci, A., Lupica, C.R., and Morales, M. (2015). Dopaminergic and glutamatergic microdomains in a subset of rodent mesoaccumbens axons. Nat. Neurosci. *18*, 386–392.

Zhou, Z., Liu, X., Chen, S., Zhang, Z., Liu, Y., Montardy, Q., Tang, Y., Wei, P., Liu, N., Li, L., et al. (2019). A VTA GABAergic neural circuit mediates visually evoked innate defensive responses. Neuron *103*, 473–488.e6.

Please cite this article in press as: Barbano et al., VTA Glutamatergic Neurons Mediate Innate Defensive Behaviors, Neuron (2020), https://doi.org/10.1016/j.neuron.2020.04.024

STAR★METHODS

KEY RESOURCES TABLE

REAGENT or RESOURCE	SOURCE	IDENTIFIER
Antibodies		
Rabbit anti-fluorogold	Millipore-Sigma	Cat# AB153-I; RRID: AB_2632408
Mouse anti-mCherry	Takara Bio	Cat# 632543; RRID: AB_2307319
Guinea pig anti-VGluT2	Frontier Institute	Cat# VGluT2-GP-Af810; RRID: AB_2341096
Rabbit anti-GFP	Frontier Institute	Cat# GFP-Rb-Af2020; RRID: AB_2571573
Rabbit anti-TH	Millipore-Sigma	Cat# AB152; RRID: AB_390204
Sheep anti-TH	Millipore-Sigma	Cat# AB1542; RRID: AB_90755
Mouse anti-GFP	Takara Bio	Cat# 632381; RRID: AB_2313808
Mouse anti-TH	Millipore-Sigma	Cat# MAB318; RRID: AB_2201528
Biotinylated goat anti-rabbit	Vector Laboratories	Cat# BA-1000; RRID: AB_2313606
Biotinylated goat anti-mouse	Vector Laboratories	Cat# BA-9200; RRID: AB_2336171
DyLight 405-AffiniPure donkey anti-sheep	Jackson ImmunoResearch Labs	Cat# 713-475-147; RRID: AB_2340740
Alexa Fluor 594-AffiniPure donkey anti-mouse	Jackson ImmunoResearch Labs	Cat# 715-585-151; RRID: AB_2340855
Alexa Fluor 647-AffiniPure donkey anti-guinea pig	Jackson ImmunoResearch Labs	Cat# 706-605-148; RRID: AB_2340476
Alexa Fluor 488-AffiniPure donkey anti-rabbit	Jackson ImmunoResearch Labs	Cat# 711-545-152; RRID: AB_2313584
Alexa Fluor 488-AffiniPure donkey anti-mouse	Jackson ImmunoResearch Labs	Cat# 715-545-150; RRID: AB_2340846
Alexa Fluor 594-AffiniPure donkey anti-rabbit	Jackson ImmunoResearch Labs	Cat# 711-585-152; RRID: AB_2340621
Alexa Fluor 647-AffiniPure donkey anti-sheep	Jackson ImmunoResearch Labs	Cat# 713-605-003; RRID: AB_2340750
DyLight 405-AffiniPure donkey anti-mouse	Jackson ImmunoResearch Labs	Cat# 715-475-151; RRID: AB_2340840
Goat anti-guinea pig IgG Fab fragment coupled to 1.4-nm gold	Nanoprobes	Cat# 2055; RRID: AB_2802149
Goat anti-rabbit IgG coupled to 1.4-nm gold	Nanoprobes	Cat# 2003; RRID: AB_2687591
Bacterial and Virus Strains		
pAAV-FLEX-taCasp3-TEVp	Yang et al., 2013	Cat# 45580; RRID: Addgene_45580
pAAV-EF1α-DIO-iChloC-2A-DsRed	Thomas Oertner	Cat# 70762; RRID: Addgene_70762
pAAV-hSyn-DIO-hM4D(Gi)-mCherry	Krashes et al., 2011	Cat# 44362; RRID: Addgene_44362
pAAV-hSyn-DIO-mCherry	Brian Roth	Cat# 50459; RRID: Addgene_50459
pAAV-Syn-Flex-GCaMP6s-WPRE-SV40	Chen et al., 2013	Cat# 100845; RRID: Addgene_100845
pAAV-EF1α-double floxed-hChR2(H134R)-mCherry-WPRE-HGHpA	Karl Deisseroth	Cat# 20297; RRID: Addgene_20297
pAAV-EF1α-double floxed-hChR2(H134R)-EYFP-WPRE-HGHpA	Karl Deisseroth	Cat# 20298; RRID: Addgene_20298
pAAV-EF1α-double floxed-EYFP-WPRE-HGHpA	Karl Deisseroth	Cat# 20296; RRID: Addgene_20296
pAAV-EF1α-DIO-eNpHR 3.0-EYFP	Gradinaru et al., 2010	Cat# 26966; RRID: Addgene_26966
pOTTC337-pAAV- EF1α-DIO-mCherry	Richie et al., 2017	Cat# 47636; RRID: Addgene_47636
pSADdeltaG-GFP-F2	Osakada et al., 2011	Cat# 32635; RRID: Addgene_32635
pAAV-CA-Flex	Watabe-Uchida et al., 2012	Cat# 38042; RRID: Addgene_38042
pAAV-EF1α-Flex-TVA-mCherry	Watabe-Uchida et al., 2012	Cat# 38044; RRID: Addgene_38044

(*Continued on next page*)

Please cite this article in press as: Barbano et al., VTA Glutamatergic Neurons Mediate Innate Defensive Behaviors, Neuron (2020), https://doi.org/10.1016/j.neuron.2020.04.024

Continued

REAGENT or RESOURCE	SOURCE	IDENTIFIER
hEF1α-LS1L-GCaMP6s	MGH Gene Delivery Technology Core	Cat# RN507
Chemicals, Peptides, and Recombinant Proteins		
Fluoro-Gold	Fluorochrome	Patent No. 4,716,905
TMT	BioSRQ	Cat# 1G-TMT-90
Lemon oil	Sigma-Aldrich	Cat# W262528-1KG-K
CNO	Sigma-Aldrich	Cat# C0832-5MG
JHU37160	Hello Bio	Cat# HB6261
Critical Commercial Assays		
HQ Silver kit	Nanoprobes	Cat# 2012
VECTASTAIN ABC-peroxidase kit	Vector Laboratories	Cat# PK-4000; RRID: AB_2336818
Durcupan ACM epoxy resin kit	Electron Microscopy Sciences	Cat# 14040
Experimental Models: Organisms/Strains		
Mouse: C57BL/6J	The Jackson Laboratory	Cat# JAX:000664; RRID: IMSR_JAX:000664
Mouse: *Slc17a6*$^{tm2(cre)Lowl}$/J (VGluT2-ires-Cre)	The Jackson Laboratory	Cat# JAX:016963
Mouse: *Slc32a1*$^{tm2(cre)Lowl}$/J (VGaT-ires-Cre)	The Jackson Laboratory	Cat# JAX:016962
Mouse: *Th*$^{tm1(cre)Te}$/J (TH-ires-Cre)	International Mouse Strain Resource	MGI:3056580
Oligonucleotides		
RNAscope probe Mm-Slc17a6	Advanced Cell Diagnostics	Cat# 319171
RNAscope probe Mm-Slc32a1	Advanced Cell Diagnostics	Cat# 319191-C3
Software and Algorithms		
ANY-maze video tracking system	Stoelting	RRID: SCR_014289; https://www.anymaze.co.uk/index.htm
GraphPad Prism 8.0	GraphPad Software	RRID: SCR_002798; https://www.graphpad.com/scientific-software/prism/
Adobe Photoshop	Adobe Systems	RRID: SCR_014199; https://www.adobe.com/products/photoshop.html
Adobe Illustrator	Adobe Systems	RRID: SCR_010279; https://www.adobe.com/products/illustrator.html
Statistica 12.0	StatSoft	RRID: SCR_014213; https://www.statsoft.de/en/statistica/statistica-software
pClamp 10.3	Molecular Devices	RRID: SCR_011323; https://www.moleculardevices.com/products/axon-patch-clamp-system/acquisition-and-analysis-software/pclamp-software-suite#gref
OriginPro 2017	OriginLab	RRID: SCR_014212; https://www.originlab.com/
MATLAB	Mathworks	RRID: SCR_001622; https://www.mathworks.com/products/matlab.html

RESOURCE AVAILABILITY

Lead contact

Further information and requests for resources and reagents should be directed to and will be fulfilled by the Lead Contact, Dr. Marisela Morales (MMORALES@intra.nida.nih.gov).

Materials availability

This study did not generate new unique reagents.

Data and code availability

All data generated and codes created during the current study are available from the lead author upon reasonable request.

EXPERIMENTAL MODEL AND SUBJECT DETAILS

Male wild-type C57BL/6J mice (n = 4) were used in anatomical FG studies. Male and female (n for each sex detailed for each specific assay) VGluT2::IRES::Cre mice (*Slc17a6*$^{tm2(cre)Lowl}$/J, in C57BL/6J background from The Jackson Laboratories, Bar Harbor, ME), VGaT::Cre mice (*Slc32a1*$^{tm2(cre)Lowl}$/J, in C57BL/6J background from The Jackson Laboratories, Bar Harbor, ME), or TH::Cre mice (*Th*$^{tm1(cre)Te}$/J, in C57BL/6J background from The Jackson Laboratories, Bar Harbor, ME) were bred in the NIDA/IRP animal facility and were used in behavioral, electrophysiological and electron microscopy experiments. Groups of 2-5 mice (weighing 20-30 g at the start of experiments) were housed in an animal vivarium maintained on a direct 12-h light-dark cycle (lights on at 7:00 am) and at a constant temperature of 23°C. Animals were kept undisturbed at least one week before the start of any experimental procedure and were handled and weighed daily to minimize handling stress during experiments. Food and water were provided *ad libitum* except during experimental sessions, unless otherwise stated. Littermates of the same sex were randomly assigned to experimental groups. All testing occurred during the light part of the mice light-dark cycle. Animal care and use were in strict accordance with institutional and international standards and were approved by the National Institute on Drug Abuse Animal Care and Use Committee. All the experiments were performed during the light phase of the diurnal cycle.

METHOD DETAILS

The coordinates used for all the stereotaxic surgeries were calculated based on Paxinos and Franklin, 2001.

Surgeries for anatomical studies

Each mouse was anesthetized with isofluorane (4%–5% for induction, 1%–2% for maintenance), placed in a stereotaxic frame and its skull was exposed and leveled. The retrograde tracer Fluoro-Gold (FG; 1% in cacodylate buffer, pH 7.5, Fluorochrome, Denver, CO) was delivered unilaterally into the VTA (AP = −3.3, ML = +0.2, DV = −4.3). FG was delivered iontophoretically through a glass micropipette (20 mm) by applying 1 μA current in 7 s pulses at 14 s intervals for 10 min. The micropipette was left in place for an additional 10 min to prevent backflow. One week following the FG injection, mice were anesthetized and perfused transcardially with fixative solution (4% paraformaldehyde, PFA) for *in situ* hybridization-immunohistochemistry.

Surgeries for EM or electrophysiology

Each mouse was anesthetized with isofluorane (4%–5% for induction, 1%–2% for maintenance), placed in a stereotaxic frame and its skull was exposed and leveled. Cre-inducible adeno-associated virus (AAV, serotype 1) coding for the light-sensitive protein channelrhodopsin-2 (ChR2) tethered to mCherry, or the enhanced yellow fluorescent protein (eYFP) under control of the EF1α promoter, were employed (NIDA IRP Optogenetics and Transgenic Technology Core, Baltimore, MD). Briefly, 300 nL of AAV1-EF1α-DIO-hChR2(H134R)-mCherry was bilaterally injected into the LHA of VGluT2-Ires-Cre mice (VGluT2-ChR2-mCherry-eYFP mice) at AP: −1.3, ML: ± 1.0, DV: −5.2. Additional 200 nL of AAV1-EF1α-DIO-eYFP was injected unilaterally into the VTA (AP: −3.4, ML: +0.3, DV: −4.4). Injections were done with a flow rate of 100 nl/min, using a UltraMicroPump with Micro 4 controller, 10 μl Nanofil syringes and 35 g needles (WPI Inc.). The needle was left in place for additional 3 min to prevent reflux. At least 8 weeks after viral injections, mice were anesthetized, and their brains were harvested for electron microscopy or electrophysiology processing (see below).

Surgeries for behavioral studies

Each mouse was anesthetized with isofluorane (4%–5% for induction, 1%–2% for maintenance), placed in a stereotaxic frame and its skull was exposed and leveled. AAV1-EF1α-DIO-hChR2(H134R)-eYFP (ChR2-eYFP mice), AAV1-EF1α-DIO-eYFP (eYFP mice) or AAV1- EF1α-DIO-eNpHR3.0-eYFP (Halo-eYFP mice) were bilaterally injected into the LHA, as previously described. In a subset of animals, 200 nL of AAV8-hSyn-DIO-hM4D(Gi)-mCherry or AAV8-hSyn-DIO-mCherry virus (Addgene, Cambridge, MA) was also injected into the VTA (AP: −3.4, ML: ± 0, DV: −4.4). Additional cohorts of VGluT2::Cre or VGaT::Cre mice were injected with 200 nL of AAV1-EF1α-Flex-taCasp3-TEVp or the control vector AAV1-EF1α-DIO-DsRed (NIDA IRP Optogenetics and Transgenic Technology Core) into the VTA. For the calcium imaging experiments, mice were injected with 200 nL of either the Cre-dependent retrograde herpes simplex virus HSV-hEF1α-LS1L-GCaMP6s (MGH Gene Delivery Technology Core, Boston, MA) or AAV1-Syn-Flex-GCaMP6s-WPRE-SV40 (Addgene) into the VTA. At least 8 weeks after viral injections, mice received intracranial optical fibers and, in pharmacology experiments, a guide cannula for VTA microinjections. For VTA photostimulation of LHA-VGluT2 fibers, mice were implanted with unilateral chronic optic fibers (200 μm diameter, BFL37-200, Thorlabs, Newton, NJ) directed just dorsal to right VTA (AP: −3.4, ML: −0.3, DV: −4.3). For VTA photoinhibition of LHA-VGluT2 fibers, mice were implanted with bilateral chronic optic fibers. For microinjection studies, a guide cannula (22 gauge, PlasticsOne, Roanoke, VA) and an optic fiber were each lowered at a 10° angle toward the right VTA (optic fiber: AP: −3.4, ML: +0.5, DV: −4.3; cannula: AP: −3.4, ML: +1.1, DV: −4.4). For calcium imaging studies, a 400 μm core optic fiber (photometry fiber, 0.48 NA) embedded in a 2.5 mm ferrule (Doric Lenses, Canada), was implanted dorsal to the right VTA (AP: −3.2, ML: −0.3, DV: −4.1) or the right LHA (AP: −1.3, ML: −1.0, DV: −5.0). One or two stainless-

steel screws and dental acrylic cement were used to anchor the optic fiber and cannula to the skull. A cap and dummy cannula were used to prevent cannula blockade. In all surgical procedures, animals were given the analgesic meloxicam (2 mg/kg) to prevent post-surgical pain or discomfort and were allowed at least 10 days of recovery before the beginning of any experimental manipulation. Body weight was measured daily after surgery to ensure proper recovery.

Histological verification

After behavioral testing, all mice were deeply anesthetized and brain tissue for immunodetection of eYFP or mCherry was processed as follows: free-floating coronal sections (30 μm) were incubated for 1 h in PB supplemented with 4% BSA and 0.3% Triton X-100. Sections were then incubated with primary antibody: mouse anti-GFP antibody (1:500, 632381, Takara, Mountain View, CA) or mouse anti-mCherry antibody (1:500, 632543, Takara), overnight at 4°C. After rinsing 3 × 10 min in PB and incubation in biotinylated goat anti-mouse antibody (1:200, Vector Laboratories) at 2 h at room temperature (RT), the sections were rinsed with PB and incubated for 1 h at room temperature in avidin-biotinylated horseradish peroxidase (1:200, ABC kit, Vector Laboratories). Sections were rinsed, and the peroxidase reaction was developed with 0.05% 3,3′-diaminobenzidine (DAB) and 0.03% H_2O_2. Sections were mounted on coated slides. Bright field images were collected with an Olympus MVX10 with 0.63 × objective (Olympus, Waltham, MA). For double fluorescence immunodetection of mCherry or eYFP and tyrosine hydroxylase (TH), free-floating coronal sections were incubated with cocktails of primary antibodies: sheep anti-TH antibody (1:1000, AB1542, Millipore, Billerica, MA) + mouse anti-GFP or mouse anti-mCherry primary antibody, overnight at 4°C. After rinsing 3 × 10 min in PB, sections were incubated in a cocktail of the corresponding fluorescence secondary antibodies (1:100, Alexa Fluor-488 or Alexa Fluor-594, Jackson Immunoresearch Laboratories, West Grove, PA) for 2 h at room temperature. After rinsing, the sections were mounted on slides. Fluorescent images were collected with an Olympus FV1000 Confocal System (Olympus). Images were taken sequentially with different lasers with 10 × (for low magnification) or 40 × (for high magnification) objectives.

In situ hybridization (ISH)

Retrograde tracing and ISH

LHA coronal free-floating sections (16 μm thickness) were incubated for 2 h at 30°C with rabbit anti-FG antibody (1:200, AB153I, Millipore, Burlington, MA) in DEPC-treated phosphate buffer (PB) with 0.5% Triton X-100 supplemented with RNasin (Promega, Madison, WI). Sections were rinsed 3 × 10 min with DEPC-treated PB and incubated in biotinylated goat anti-rabbit antibody (1:200, Vector Laboratories, Burlingame, CA) for 1 h at 30°C. Sections were rinsed with DEPC-treated PB and then transferred to 4% PFA. Sections were rinsed with DEPC-treated PB, incubated for 10 min in PB containing 0.5% Triton X-100, rinsed with PB, treated with 0.2 N HCl for 10 min, rinsed with PB and then acetylated in 0.25% acetic anhydride in 0.1 M triethanolamine, pH 8.0, for 10 min. Sections were rinsed with PB, and postfixed with 4% PFA for 10 min. Before hybridization, and after a final rinse with PB, the sections were incubated in hybridization buffer for 2 h at 55°C (50% formamide, 10% dextran sulfate, 5 × Denhardt's solution, 0.62 M NaCl, 50 mM DTT, 10 mM EDTA, 20 mM PIPES, pH 6.8, 0.2% SDS, 250 mg/ml salmon sperm DNA, 250 g/ml tRNA). Sections were hybridized for 16 h at 55°C in hybridization buffer containing [^{35}S]- and [^{33}P]-labeled single-stranded antisense VGluT2 (nucleotides 317-2357; GenBank: NM-053427) probes at 10^7 cpm/ml. Sections were treated with 4 mg/ml RNase A at 37°C for 1 h and washed with 1 × saline-sodium citrate, 50% formamide at 55°C for 1 h and with 0.1 × saline-sodium citrate at 68°C for 1 h. Then, sections were rinsed with PB and incubated for 1 h at room temperature in avidin-biotinylated horseradish peroxidase (1:100, ABC kit, Vector Laboratories). Sections were rinsed, and the peroxidase reaction was developed with 0.05% 3,30-diaminobenzidine (DAB) and 0.03% H_2O_2. Sections were mounted on coated slides. Sections were then photographed under bright-field illumination for FG staining. Slides were dipped in Ilford K.5 nuclear tract emulsion (1:1 dilution in double-distilled water, Polysciences, Warrington, PA) and exposed in the dark at 4°C for 4 weeks before development. Images were taken with bright-field or epiluminescence microscopy using an Olympus BX51 microscope. Neurons were observed within each traced region at × 20 objective lenses and marked electronically.

c-Fos immunolabeling and ISH

Midbrain coronal free-floating sections (16 μm) were incubated for 10 min in PB containing 0.5% Triton X-100, rinsed three times (10 min each time) with PB, treated with 0.2 N HCl for 10 min, rinsed three times (10 min each time) with PB, and then acetylated in 0.25% acetic anhydride in 0.1 M triethanolamine, pH 8.0, for 10 min. Sections were rinsed three times (10 min each time) with PB and post-fixed with 4% PFA for 10 min. Before hybridization and after a final rinse with PB, the sections were incubated in hybridization buffer (50% formamide, 10% dextran sulfate, 5 × Denhardt's solution, 0.62 M NaCl, 50 mM DTT, 10 mM EDTA, 20 mM PIPES, pH 6.8, 0.2% SDS, 250 μg/ml salmon sperm DNA, 250 μg/ml tRNA) for 2 h at 55°C. Sections were hybridized for 16 h at 55°C in hybridization buffer containing [^{35}S]- and [^{33}P]-labeled single-stranded antisense rat *VGluT2* probes at 10^7 cpm/mL together with the single-stranded rat digoxigenin (DIG)-labeled antisense probe for mouse GABA vesicular transporter (*VGaT,* nucleotides 1–2814, GenBank: BC_052020). Sections were treated with 4 μg/ml RNase A at 37°C for 1 h, washed with 1 × SSC, 50% formamide at 55°C for 1 h, and the washed with 0.1 × SSC at 68°C for 1 h. After the last SSC wash, to develop DIG signal, sections were incubated with an alkaline phosphatase–conjugated antibody against DIG (Roche Applied Science; Indianapolis, IN) for 3 h at RT; alkaline phosphatase reaction was developed with nitro blue tetrazolium and 5-bromo-4-chloro-3-indolyl phosphate (Life Technologies; Gaithersburg, MD), yielding a purple reaction product. Sections were then photographed under bright-field illumination. All sections were rinsed with PB and incubated for 1 h in PB supplemented with 4% BSA and 0.3% Triton X-100. This was followed by overnight incubation at 4°C with a rabbit anti–c-Fos (1:300, Santa Cruz Biotechnology, SC-52). After being rinsed three

times for 10 min each time in PB, sections were processed with an ABC kit (Vector Laboratories). The material was incubated for 2 h at room temperature in a 1:200 dilution of the biotinylated secondary antibody, rinsed with PB, and incubated with avidin-biotinylated horseradish peroxidase for 1 h. Sections were rinsed, and the peroxidase reaction was then developed with 0.05% 3,3-diaminobenzidine-4 HCl and 0.03% hydrogen peroxide (H_2O_2). The sections were mounted on coated slides. Sections were then photographed under bright-field illumination for c-Fos staining. Slides were dipped in Ilford K.5 nuclear tract emulsion (Polysciences; 1:1 dilution in double-distilled water) and exposed in the dark at 4°C for 4 weeks before development. Sections were viewed, analyzed, and photographed with bright-field or epiluminescence microscopy using an Olympus BX51 microscope. Neurons were observed within each VTA region at high power (20 × objective lenses) and marked electronically.

RNAscope

The remaining *in situ* hybridization experiments detected transcripts encoding VGluT2, VGaT or TH mRNA and immunodetection of TH (1:1000, MAB318, Millipore, Burlington, MA) or GFP (1:500, 632381, Takara Bio USA, Inc. Mountain View, CA) using RNAscope combined with immunolabeling. Coronal free-floating sections (VTA, 16 μm) were processed for immunolabelling as described above, and incubated with secondary Donkey anti-Mouse Alexa Fluor 488 or Donkey anti-Mouse Alexa Fluor 594 (1:100, 715-545-151 or 715-585-151, Jackson ImmunoResearch, West Grove, PA) for 1 h at 30°C. Sections were rinsed with DEPC-treated PB and then were mounted onto Fisher SuperFrost slides and dried overnight at 60°C. RNAscope *in situ* hybridization was performed according to the manufacturer's instructions. Briefly, sections were treated with heat and protease digestion followed by hybridization with a mixture containing target probes to mouse VGluT2 (319171, Advanced Cell Diagnostics, Newark, CA), VGaT (319191-C3, Advanced Cell Diagnostics, Newark, CA), or TH (317621-C2, Advanced Cell Diagnostics, Newark, CA). Additional sections were hybridized with the bacterial gene DapB as a negative control, which did not exhibit fluorescent labeling. VGluT2 and VGaT were detected by either Atto 550 or Alexa 488. Some sections were also labeled with DAPI (320850, Advanced Cell Diagnostics, Newark, CA). RNAscope *in situ* hybridization sections were viewed, analyzed, and photographed with an Olympus FV1000 confocal microscope or a Keyence BZ-X800 microscope. Negative control hybridizations showed negligible fluorophore expression. Neurons were counted when the stained cell was at least 5 μm in diameter. Pictures were adjusted to match contrast and brightness by using Adobe Photoshop (Adobe Systems). The number of mice (n = 3/group; 3 sections/mouse) analyzed was based on previous studies in our lab using radioactive detection of VGluT2 mRNA from rat VTA neurons (Yamaguchi et al., 2011).

Electron and confocal microscopy

Electron microscopy

Vibratome tissue sections were rinsed and incubated with 1% sodium borohydride to inactivate free aldehyde groups, rinsed and then incubated with blocking solution. Sections were then incubated with primary antibodies [mouse anti-mCherry (1:1,000, Takara, #632543), guinea pig anti-VGluT2 (1:500, Frontier Institute, VGluT2-GP-Af810) and rabbit anti-GFP (1:2000, Frontier Institute, GFP-Rb-Af2020)]; or primary antibodies [mouse anti-mCherry (1:1,000, Takara, #632543), guinea pig anti-VGluT2 (1:500, Frontier Institute, VGluT2-GP-Af810) and rabbit anti-TH (1:1000, Millipore Sigma, AB152)]. All primary antibodies were diluted with 1% normal goat serum (NGS), 4% BSA in PB supplemented with 0.02% saponin and incubations were for 24 h at 4°C. Sections were rinsed and incubated overnight at 4°C in the corresponding secondary antibodies. Sections were rinsed in PB, and then in double-distilled water, followed by silver enhancement of the gold particles with the Nanoprobe Silver Kit (2012, Nanoprobes) for 7 min at room temperature. Next, sections were incubated in avidin-biotinylated horseradish peroxidase complex in PB for 2 h at room temperature and washed. Peroxidase activity was detected with 0.025% 3,3′-diaminobenzidine (DAB) and 0.003% H_2O_2 in PB for 5-10 min. Sections were rinsed with PB and fixed with 0.5% osmium tetroxide in PB for 25 min, washed in PB, followed by double distilled water, and then contrasted in freshly prepared 1% uranyl acetate for 35 min. Sections were dehydrated through a series of graded alcohols and with propylene oxide. Afterward, they were flat embedded in Durcupan ACM epoxy resin (14040, Electron Microscopy Sciences). Resin-embedded sections were polymerized at 60°C for 2 days. Sections of 60 nm were cut from the outer surface of the tissue with an ultramicrotome UC7 (Leica Microsystems) using a diamond knife (Diatome). The sections were collected on formvar-coated single slot grids and counterstained with Reynolds lead citrate. Sections were examined and photographed using a Tecnai G2 12 transmission electron microscope (Fei Company) equipped with the OneView digital micrograph camera (Gatan).

Ultrastructural analysis

Serial ultrathin sections of the VTA (bregma −2.92 mm to −3.64 mm) from 3 male VGluT2-ChR2-mCherry-eYFP mice were analyzed. Synaptic contacts were classified according to their morphology and immunolabel and photographed at a magnification of 6,800-13,000 ×. The morphological criteria used for identification and classification of cellular components or type of synapse observed in these thin sections were as previously described (Peters et al., 1991). In the serial sections, a terminal containing greater than 5 immunogold particles was considered as immunopositive terminal. Pictures were adjusted to match contrast and brightness by using Adobe Photoshop (Adobe Systems Incorporated, Seattle, WA). This experiment was successfully repeated three times. Electron microscopy and confocal analysis quantification were blinded.

Fluorescence microscopy

Free floating coronal sections (40 μm) from VGluT2-ChR2-mCherry-eYFP mice (n = 4) were incubated for 1 h in PB supplemented with 4% BSA and 0.3% Triton X-100. Sections were then incubated with cocktails of primary antibodies: mouse anti-mCherry (1:500) + guinea pig anti-VGluT2 (1:500) + rabbit anti-GFP (1:2000) + sheep anti-TH (1:1000, Millipore Sigma, AB1542), overnight

at 4°C. After rinsing 3 × 10 min in PB, sections were incubated in a cocktail of the corresponding fluorescence secondary antibodies: DyLight-405-donkey anti-sheep + Alexa Fluor-488-donkey anti-rabbit + Alexa Fluor-594-donkey anti-mouse + Alexa Fluor-647-donkey anti-guinea pig for 2 h at room temperature. After rinsing, sections were mounted on slides. Fluorescent images were collected with an Olympus FV1000 Confocal System (Olympus). Images were taken sequentially with different lasers with 10 × and 100 × oil immersion objectives and Z axis stacks were collected at 0.2 μm. This experiment was successfully repeated three times.

Electrophysiology

Eight weeks after virus injection, VGluT2-Ires-Cre mice carrying AAV1-DIO-ChR2-mCherry in LHA and AAV1-DIO-eYFP in VTA (n = 11) were anesthetized with chloral hydrate (8 mg/kg) and perfused with ice-cold aCSF, saturated with 95% O_2 and 5% CO_2, and modified to contain (in mM): 92 NMDG, 20 HEPES, 25 glucose, 30 $NaHCO_3$, 1.2 NaH_2PO_4, 2.5 KCl, 5 sodium ascorbate, 3 sodium pyruvate, 2 thiourea, 10 $MgSO_4$ and 0.5 $CaCl_2$. Brains were then removed quickly, placed in this same solution on a VT-1200 vibratome (Leica, Nussloch, Germany), and sectioned through the VTA in horizontal slices (200 μm thickness). The slices were placed in a holding chamber filled with the same solution, but held at 32°C. After 15 min, slices were transferred to a holding chamber containing room temperature aCSF modified to contain (in mM): 92 NaCl, 20 HEPES, 25 glucose, 30 $NaHCO_3$, 1.2 NaH_2PO_4, 2.5 KCl, 5 sodium ascorbate, 3 sodium pyruvate, 2 thiourea, 1 $MgSO_4$, 2 $CaCl_2$. For recordings, slices were transferred to a chamber superfused with 32°C aCSF modified to contain (in mM): 125 NaCl, 2.5 KCl, 1.25 NaH_2PO_4, 1 $MgCl_2$, 2.4 $CaCl_2$, 26 $NaHCO_3$ and 11 glucose. Electrodes (3-6MΩ) were backfilled with an internal solution containing (in mM): 140 potassium gluconate, 2 NaCl, 1.5 $MgCl_2$, 10 HEPES, 4 Mg-ATP, 0.3 Na_2-GTP, 10 Naphosphocreatine, 0.1 EGTA and 0.2% biocytin (pH 7.2; 280-290 mOsm). Cells were visualized on an upright microscope using infrared differential interference contrast video microscopy. Whole-cell voltage-clamp or current clamp recordings were made using a MultiClamp 700B amplifier (2 kHz low-pass Bessel filter and 10 kHz digitization) with pClamp 10.3 software (Molecular Devices, Sunnyvale, CA). VTA VGluT2 neurons were identified by expression of eYFP. Neurons were voltage clamped at −60 mV. Series resistance (10-30 MΩ) was monitored with a 5 mV hyperpolarizing pulse (50 ms) given every 10 s, and only recordings that remained stable over the period of data collection were used. A 200 μm core optical fiber, coupled to a diode-pumped solid-state laser, was positioned just above the slice and aimed at the recorded cell. Optically-evoked EPSCs were obtained every 10 s with pulses of 473 nm wavelength light (8 mW, 5-10 ms). After evoking EPSC, bicuculline (10 μM) or CNQX (10 μM) were added in the perfusion aCSF to block GABA A or AMPA receptors. The peak amplitude of EPSCs was measured with the average of 30 consecutive traces.

Fiber photometry

For all recordings, GCaMP6s was excited at two wavelengths (490nm, calcium-dependent signal and 405 nm isosbestic control; Lerner et al., 2015) by amplitude modulated signals from two light-emitting diodes reflected off dichroic mirrors and coupled into the photometry fiber. Signals emitted from GCaMP6s and its isosbestic control channel then returned through the same optic fiber and were acquired using a femtowatt photoreceiver (Model 2151; Newport; Irvine, CA), digitized at 1kHz, and then recorded by a real-time signal processor (RZ5D; Tucker Davis Technologies, TDT, Alachua, FL) running the Synapse software suite (TDT). Analysis of the resulting signal was then performed using custom-written MATLAB (Natick, MA) scripts. Changes in fluorescence across the experimental session (ΔF/F) were calculated by smoothing signals from the isosbestic control channel (Lerner et al., 2015), scaling the isosbestic control signal by regressing it on the smoothed GCaMP signal, and then generating a predicted 405nm signal using the linear model generated during the regression. Calcium independent signals on the predicted 405nm channel were then subtracted from the raw GCAMP signal to remove movement, photo-bleaching, and fiber bending artifacts. Signals from the GCaMP channel were then scored to normalize changes in fluorescence across animals (normalized ΔF/F). Peri-event time-locked histograms were then created by averaging changes in fluorescence (ΔF/F) across repeated trials during windows encompassing behavioral events of interest. Video recordings synchronized with neuronal acquisition clocks were acquired using an RV2 video system at 20 Hz (TDT) or using the Synapse webcam acquisition system at 20 Hz.

Behavioral studies

Laser photostimulation and photoinhibiton parameters

Photostimulation was administered with a frequency of 20 Hz, a pulse duration of 10 ms and an intensity of 8 mW. Photoinhibition was continuously administered, with an intensity of 8 mW.

Looming and shelter tests

eYFP, ChR2-eYFP or Halo-eYFP mice (12 females, 16 males) were habituated for three days to an open field arena made of acrylic with opaque walls and non-reflective base plate (40 × 40 × 35 cm; AnyBox, Stoelting, Wood Dale, IL) for 6 min, without being connected to the fiber optic cable and laser. The experiment was then divided in a pretest and a test phases, conducted on different days, and lasted 6 min. During the first 3 min of either pretest or test, VTA photostimulation or photoinhibition was off; during the last 3 min of the pretest, VTA photostimulation or photoinhibition was also off but during the last 3 min of the test session, VTA photostimulation or photoinhibition was on. A looming stimulus (a handle ending on a black circle, 16.5 cm of diameter) was mechanically descended above (but without touching) the arena, twice per min during the last 3 min of either the pretest or the test. Total duration of the looming stimulus administration calculated for all the experiments was 1.14 ± 0.03 s, with a range of 1-1.5 s. Testing time was divided in

Please cite this article in press as: Barbano et al., VTA Glutamatergic Neurons Mediate Innate Defensive Behaviors, Neuron (2020), https://doi.org/10.1016/j.neuron.2020.04.024

60 s trials and the average speed of the mice was calculated for the first 3 min (3 60 s trials) of either pretest or test (the phase without looming stimulus presentation). A run was counted every time the mice showed an increase in the average speed above the value calculated. The total number of runs was measured. For speed changes analyses, the second part of either pretest or test (4 to 6 min) was divided in 10 s trials and the exact moment the looming stimulus was above the arena was calculated and assigned to its corresponding 10 s trial. The speed during that 10 s trial (stimulus trial, S), as well as the 10 s trials before (pre-stimulus trial, Pre-S) and after (post-stimulus trial, Post-S) was calculated for each mouse.

The looming experiment was repeated with a cardboard shelter (8 × 10.5 × 11 cm) located in one of the corners, against the wall of the arena. The total number of runs, as well as the time spent inside the shelter, was recorded. Half of eYFP mice received VTA photostimulation and the other half received VTA photoinhibition. Given that the results were not significantly different, the data from all eYFP mice were pooled together.

The looming test without shelter was carried out as described for mice in which VTA-VGluT2 (5 females, 11 males) or VGaT (16 males) neurons have been destroyed by a cell ablation approach. Additional looming tests (8-10 trials) were conducted while Ca^{2+} activity was measured by *in vivo* photometry in the LHA (2 females, 5 males) or the VTA (4 females, 8 males) of VGluT2::Cre mice. Frame by frame timestamps were overlayed onto recorded video files by Avidemux v2.6 (Greenwood Village, CO). For the analysis of photometry data, the peak ΔF/F and area under the curve (AUC) for the baseline window were collected from −5 s to 0 s relative to the looming stimulus onset (when the disk was immediately above the arena). The same measures were collected for the onset window (from 0 s to 5 s relative to the looming stimulus onset) and were used for statistical analysis.

Odor tests

The odors were diluted in propanediol (Sigma Aldrich, St. Louis, MO). All mice were habituated to the testing environment for three days before any experimental manipulation.

During testing, mice in which VTA-VGluT2 (5 females, 11 males) or VGaT (16 males) neurons have been destroyed by a cell ablation approach were individually placed in a chamber (20 × 18 × 35 cm) with a small (5 cm) exit area containing a glass culture dish (3.8 cm diameter). A circular filter paper (15 mm diameter) containing 5 μl of 10% of the synthetic predator odor trimethylthiazoline (TMT, SRQ-Bio, Sarasota, FL) was placed inside the culture dish and the latency to escape the chamber was measured.

For the photometry studies involving odor presentations, VGluT2::Cre mice expressing GCaMP6s in either the LHA (4 females, 5 males) or the VTA (4 females, 8 males) were placed on a plastic cage (10 × 23 × 15 cm) enclosed in an operant chamber equipped with an odor generator (Knosys Olfactometers Inc., Lutz, FL). Odors (lemon, Sigma-Aldrich, W262528-1KG-K or TMT, 10% in filtered air) were pseudo-randomly presented (10 lemon trials and 10 TMT trials) for 5 s, with an inter-trial interval (ITI) of 15-20 min. During the ITI, the air inside the chamber was replaced with filtered air and extracted by a build-in fan (Knosys Olfactometers Inc.). The experimental plastic cage was thoroughly cleaned with ethanol 70% between trials. The normalized peak ΔF/F and AUC for the baseline window were collected from −5 s to 0 s relative to the odor presentation. The same measures were collected for the odor window (from 0 s to 5 s relative to the odor presentation) and were used for statistical analysis.

For chemogenetic inhibition of VTA-VGluT2 neurons, mice (4 females, 21 males) expressing hM4D-mCherry in the VTA were intraperitoneally injected with vehicle (1% DMSO in saline) or CNO (3 mg/kg in vehicle) 30 min before testing, in a counterbalanced sequence, after which TMT (10%) was presented. The latency to escape the chamber was measured. In a different set of chemogenetic inhibition experiments, VGluT2::Cre mice expressing mCherry or hM4D-mCherry in the VTA (2 females, 10 males) were intraperitoneally injected with vehicle (saline) or JHU 37160 (J60, 0.1 mg/kg, Hello Bio, Princeton, NJ) 30 min before presentation of TMT, in a counterbalanced sequence. The latency to escape the chamber was measured. A new cohort of VGluT2::Cre mice expressing hM4D-mCherry in the VTA (2 females, 4 males) received intra-VTA administration of J60 (200 nl, 0.1 μg/μl, in aCSF) as previously described, 10 min before the presentation of a glass culture dish (3.8 cm diameter) containing walnut-based cat litter (Naturally Fresh, Corning, CA). The clean cat litter was imbibed with either tap water or the urine of 2 domestic cats. The latency to escape the chamber with the glass dish was measured.

In additional experiments, eYFP, ChR2-eYFP or Halo-eYFP mice (13 females, 11 males) were connected to the fiber optic cable and laser, and individually placed in the chamber previously described. Five μl of 10% lemon oil or 10% TMT were presented and VTA photostimulation (20 Hz) or photoinhibition (continuous light) were administered. The latency to escape the chamber was measured.

For chemogenetic inhibition of VTA-VGluT2 neurons after optogenetic activation of LHA-VGluT2 neurons, eYFP and ChR2-eYFP mice (4 females, 21 males) were intraperitoneally injected with vehicle (1% DMSO in saline) or CNO (3 mg/kg in vehicle) 30 min before testing, in a counterbalanced sequence. Only lemon odor was presented. VTA photostimulation (20 Hz) was administered and the latency to escape the chamber was measured.

Forced swimming test

eYFP, ChR2-eYFP or Halo-eYFP mice (13 females, 11 males) were connected to the fiber optic cable and laser, and individually placed in a glass beaker filled with 1 l warm tap water (37°C). The test lasted 4 min. During the first 2 min VTA photostimulation or photoinhibition was off, during the last 2 min VTA photostimulation or photoinhibition was on. Total distance traveled, average and maximum speed and time immobile were recorded. A detailed analysis conducted every 30 s for both laser-off and laser-on epochs was also conducted. Half of eYFP mice received VTA photostimulation and the other half received VTA photoinhibition. Given that the results were not significantly different, the data from all eYFP mice were pooled together.

Please cite this article in press as: Barbano et al., VTA Glutamatergic Neurons Mediate Innate Defensive Behaviors, Neuron (2020), https://doi.org/10.1016/j.neuron.2020.04.024

Feeding and tail grab tests

For the photometry studies involving food presentation, VGluT2::Cre mice expressing GCaMP6s in the VTA (5 females, 4 males) were food-restricted at 90% of their free-feeding weight and presented with a pre-weighed amount of standard chow (SC, 2018 Teklad Global 18% protein rodent diet, Harlan, Indianapolis, IN: 18.6% protein, 44.2% carbohydrate and 6.2% fat, with a caloric content of 3.1 kcal/g) or chocolate-flavored sucrose pellets (CP, F0025 Dustless Precision Pellets, Bioserv, Flemington, NJ: 0.2% protein, 94.3% carbohydrate and 0.6% fat, with a caloric content of 3.83 kcal/g) in their home cage. Ca^{2+} activity was measured by *in vivo* photometry during 10-20 min. During this experiment, mice were lightly grabbed from the tail and lifted from the group to a height of 15 cm. Timestamps indicating the onset of a feeding bout (independent feeding bouts were counted after 3 s without eating elapsed) or of the tail grab were included in the Synapse recorded file for each mouse. The normalized peak $\Delta F/F$ and AUC for the baseline window were collected from −5 s to 0 s relative to the onset of a feeding bout or of the tail grab. The same measures were collected for the consumption or tail grab windows (from 0 s to 5 s relative to the onset) and were used for statistical analysis. Each food was presented either in the morning or the afternoon and the total amount of food eaten was calculated at the end of the experiment.

Open field test

The same open field arena used in the looming experiments was divided into the central area (20 × 20 cm) and the periphery area. ChR2-eYFP and eYFP male mice were habituated to the testing environment for 2 hours. Mice were connected to the fiber optic cable and laser, but no photostimulation was delivered. Next day, three 2-min tests were consecutively conducted: before, during and after VTA photostimulation (10 ms, 8 mW, 20 Hz); and time spent in the central and periphery areas was recorded.

For all the experiments, the order of the food, laser or no laser days, as well as the pharmacology injections was counterbalanced across days, with half the mice receiving laser/no laser (SC/CP or saline/J60-CNO) and the other half receiving no laser/laser (CP/SC or J60-CNO/saline) on any given day. For the behavioral tests, the position of the animal was monitored via an overhead closed-circuit camera interfaced with video tracking software (AnyMaze, Stoelting). Fiber optic cables were attached via FC/PC connector to 473 nm or 532 nm lasers (OEM/Opto Engine LLC, Midvale, UT) for photostimulation or photoinhibition, respectively.

At the end of each behavioral experiment, mice were anesthetized and perfused with 4% paraformaldehyde in 0.1 M PB, and coronal sections of 30 μm were cut with a cryostat (CM3050 S, Leica, Buffalo Grove, IL) and prepared, as reported previously (Qi et al., 2014).

QUANTIFICATION AND STATISTICAL ANALYSIS

The number of mice (“n”) used in each group or condition is described either in the main text or in the legend of each figure. No statistical methods were used to predetermine sample size, but sample sizes are consistent with those reported in previous publications in the field and in our laboratory. In optogenetic experiments, mice with fiber tip placement outside of the targeted structure were excluded from the analysis. All attempts at replication were successful. All experiments were conducted in a blind manner such that assays were carried out and analyzed without knowledge of the experimental group of the animal under study. Results are presented as mean ± SEM. Behavioral data were analyzed using a Student’s t test, in the case where two variables were to be compared, and using a multifactorial analysis of variance (MANOVA) with group (i.e. eYFP, ChR2-eYFP, Halo-eYFP) as the between-subjects factor, and trials, intracerebral injections, phases of testing, etc, as within-subject factors, in the case where more than two variables were to be compared. When the same mice were tested under different conditions or when different brain subnuclei were analyzed in the same mouse, a repeated-measures ANOVA was used instead. For significant overall interactions, further analyses of partial interactions were carried out. *Post hoc* analyses were performed using the Newman-Keuls test (the Dunnett test in the case of electrophysiology studies or the Bonferroni test in the case of photometry studies) when the initial *p-value* was significant. A result was considered significant if $p < 0.05$. All data were analyzed using Statistica software (Statsoft Inc., Tulsa, OK) or the statistical computing language R, in the case of photometry studies.

Neuron, Volume *107*

Supplemental Information

VTA Glutamatergic Neurons Mediate Innate Defensive Behaviors

M. Flavia Barbano, Hui-Ling Wang, Shiliang Zhang, Jorge Miranda-Barrientos, David J. Estrin, Almaris Figueroa-González, Bing Liu, David J. Barker, and Marisela Morales

Supplemental Table 1. Frequency of neurons co-expressing FG immunoreactivity and VGluT2 mRNA in the LHA, related to Figure 3

Bregma (in mm)	Subject	Percentage of LHA neurons co-expressing FG immunoreactivity and VGluT2 mRNA	Percentage of LHA neurons expressing FG immunoreactivity but lacking VGluT2 mRNA
-1.22	1	63.64% (*n* = 7)	36.36% (*n* = 4)
	2	31.82% (*n* = 7)	68.18% (*n* = 15)
	3	45.83% (*n* = 11)	54.17% (*n* = 13)
	4	53.33% (*n* = 16)	46.67% (*n* = 14)
	Mean ± S.E.M.	**48.66 ± 6.69% (*n* = 41)**	**51.34 ± 6.69% (*n* = 46)**
-1.58	1	42.86% (*n* = 15)	57.14% (*n* = 20)
	2	33.33% (*n* = 6)	66.67% (*n* = 12)
	3	29.87% (*n* = 23)	70.13% (*n* = 54)
	4	31.34% (*n* = 21)	68.66% (*n* = 46)
	Mean ± S.E.M.	**34.35 ± 2.92% (*n* = 65)**	**65.65 ± 2.92% (*n* = 132) ***
-1.94	1	36.0% (*n* = 9)	64.0% (*n* = 16)
	2	27.8% (*n* = 5)	72.2% (*n* = 13)
	3	40.0% (*n* = 22)	60.0% (*n* = 33)
	4	45.1% (*n* = 32)	54.9% (*n* = 39)
	Mean ± S.E.M.	**37.21 ± 3.65% (*n* = 68)**	**62.79 ± 3.65% (*n* = 101) #**

Neurons co-expressing FG immunoreactivity and VGluT2 mRNA were counted in 16 µm thick sections from 4 different mice (subject 1, 2, 3 and 4). *n* = total number of FG-positive neurons expressing or lacking VGluT2 mRNA in the LHA. A tendency for medial (bregma -1.58) and caudal (bregma -1.94) occurrence of LHA neurons expressing FG immunoreactivity but lacking VGluT2 mRNA was observed (bregma x phenotype: $F_{(2,6)}$=3.93, P=0.08, ANOVA with Newman-Keuls *post hoc* test). * P<0.05, # P=0.06, against percentage of LHA neurons co-expressing FG immunoreactivity and VGluT2 mRNA.

Supplemental Table 2. Distribution of neurons co-expressing c-Fos immunoreactivity and VGluT2 mRNA within the different VTA subnuclei, related to Figure 4

VTA subnucleus	Subject	Number of VTA neurons co-expressing c-Fos immunoreactivity and VGluT2 mRNA
VTAr	1	46
	2	55
	3	40
	Mean ± S.E.M.	**47 ± 4.36**
PBP	1	75
	2	42
	3	48
	Mean ± S.E.M.	**55 ± 10.15**
PN	1	3
	2	5
	3	10
	Mean ± S.E.M.	**6 ± 2.08 ****
RLi	1	45
	2	34
	3	39
	Mean ± S.E.M.	**39.33 ± 3.18**
IF	1	27
	2	18
	3	21
	Mean ± S.E.M.	**22 ± 2.65 ***

Neurons co-expressing c-Fos immunoreactivity and VGluT2 mRNA were counted in 16 µm thick sections from 3 different ChR2-eYFP mice (subjects 1, 2, and 3). Neurons co-expressing c-Fos immunoreactivity and VGluT2 mRNA were differentially distributed within the VTA (subnucleus: $F_{(4,8)}$=14.55, P<0.001, ANOVA with Newman-Keuls *post hoc* test). * P<0.05, ** P<0.01, against number of neurons within the RLi.

Supplemental Table 3. Average speed (m/s) during the 10-s trial in which the looming stimulus was presented, related to Figure 5

Group	Looming presentation	Pretest	Test
eYFP (n = 10)	1	0.069 ± 0.011	0.057 ± 0.018
	2	0.047 ± 0.009	0.051 ± 0.024
	3	0.048 ± 0.010	0.051 ± 0.015
	4	0.050 ± 0.013	0.064 ± 0.027
	5	0.044 ± 0.013	0.044 ± 0.017
	6	0.051 ± 0.014	0.037 ± 0.015
ChR2-eYFP (n = 10)	1	0.076 ± 0.010	0.137 ± 0.029
	2	0.045 ± 0.007	0.121 ± 0.019
	3	0.042 ± 0.013	0.157 ± 0.035
	4	0.065 ± 0.018	0.132 ± 0.024
	5	0.035 ± 0.012	0.143 ± 0.021
	6	0.054 ± 0.010	0.105 ± 0.021
Halo-eYFP (n = 8)	1	0.067 ± 0.014	0.032 ± 0.010
	2	0.044 ± 0.013	0.024 ± 0.007
	3	0.038 ± 0.010	0.029 ± 0.013
	4	0.041 ± 0.011	0.016 ± 0.007
	5	0.045 ± 0.011	0.044 ± 0.024
	6	0.052 ± 0.006	0.036 ± 0.009

Average speed was calculated for each of the looming stimulus presentation during pretest or test, showing that the speed of ChR2-eYFP mice was higher during the test than the pretest, and it was also higher than the speed of the other groups for either test or pretest. While the triple interaction between group, phase of test and event was not significant ($F_{(10,125)}$=0.44, P=0.093, ANOVA with Newman-Keuls *post hoc* test); the main effect group (ChR2-eYFP > eYFP = Halo-eYFP; $F_{(2,25)}$=13.21, P<0.001, ANOVA with Newman-Keuls *post hoc* test), phase of test (test > pretest; $F_{(1,25)}$=5.12, P<0.05, ANOVA with Newman-Keuls *post hoc* test) and the interaction between those 2 factors ($F_{(2,25)}$=11.19, P<0.001, ANOVA with Newman-Keuls *post hoc* test) was significant.

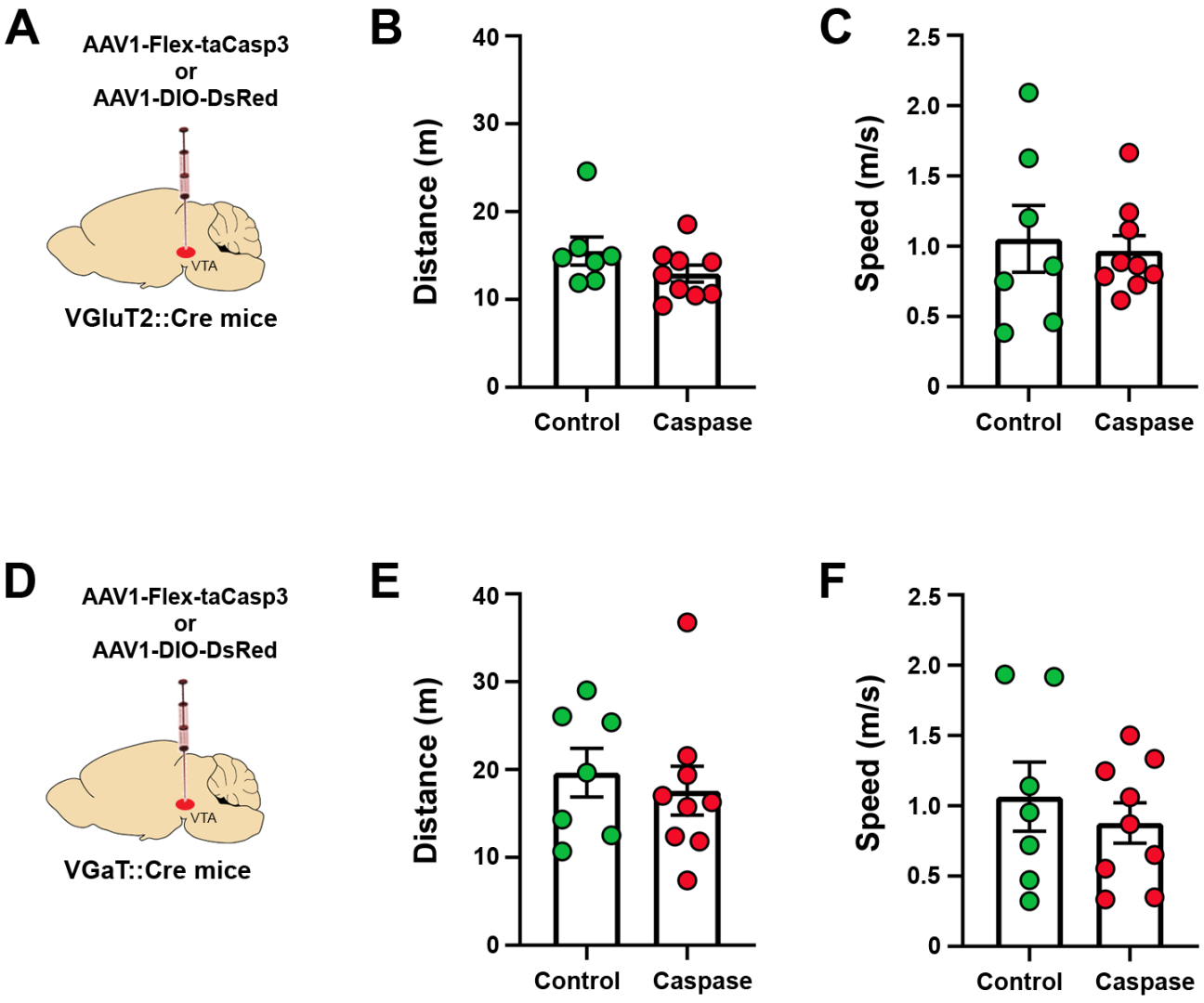

Figure S1. Ablation of VTA-VGluT2 or VGaT neurons does not modify motor behavior, related to Figure 1. (A) Diagram of VTA viral injections. **(B)** Total distance travelled was not modified by ablation of VTA-VGluT2 neurons (control, n=7; caspase, n=9; $t_{(14)}$=1.43, P=0.17, t test; data represent mean ± SEM). **(C)** Speed was not modified by ablation of VTA-VGluT2 neurons (control, n=7; caspase, n=9; $t_{(14)}$=0.36, P=0.72, t test; data represent mean ± SEM). **(D)** Diagram of VTA viral injections. **(E)** Total distance travelled was not modified by ablation of VTA-VGluT2 neurons (control, n=7; caspase, n=9; $t_{(14)}$=0.52, P=0.61, t test; data represent mean ± SEM). (**F**) Speed was not modified by ablation of VTA-VGluT2 neurons (control, n=7; caspase, n=9; $t_{(14)}$=0.69, P=0.50, t test; data represent mean ± SEM).

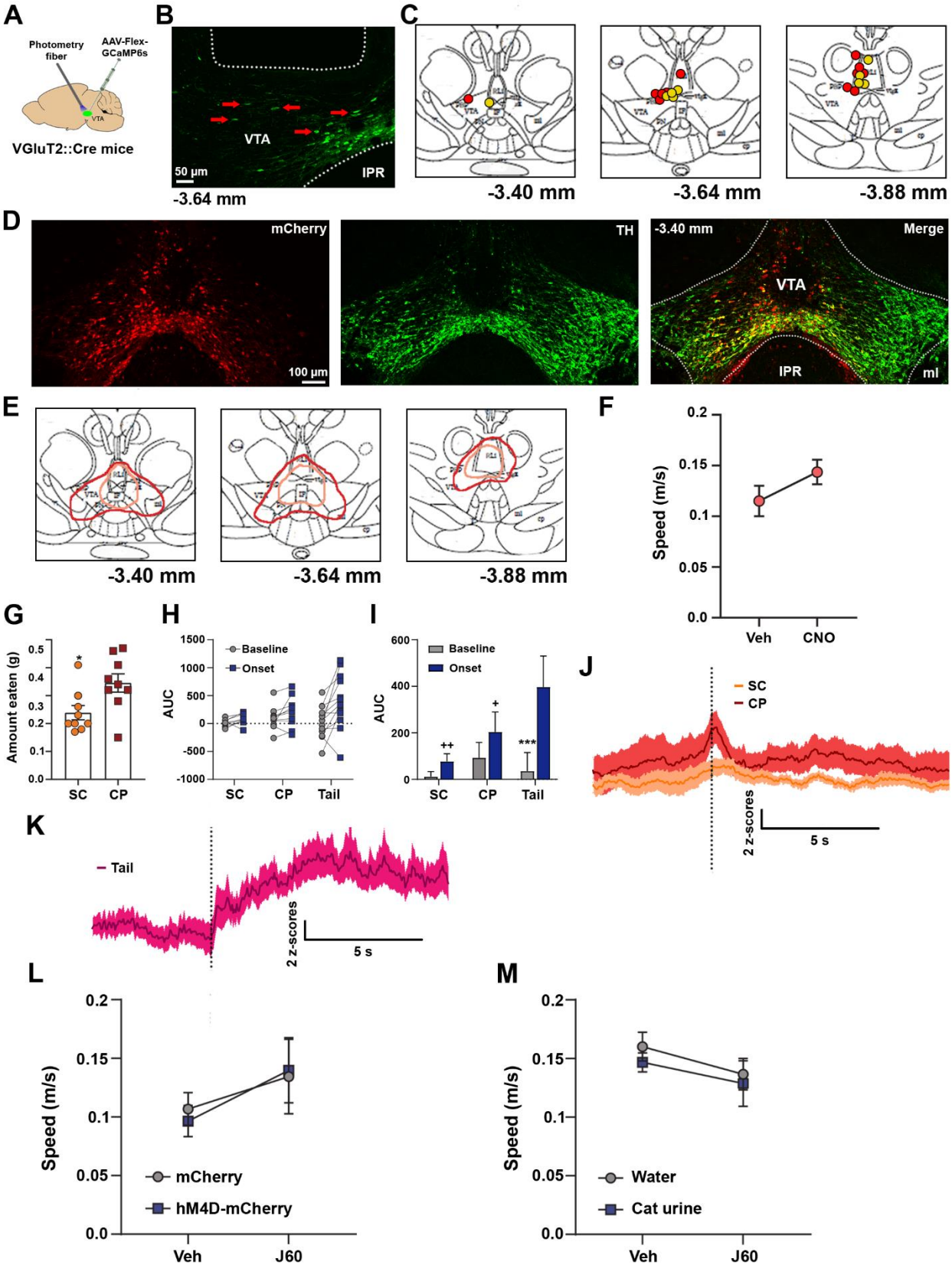
A
Photometry fiber
AAV-Flex-GCaMP6s
VTA
VGluT2::Cre mice
B
VTA
50 µm
IPR
-3.64 mm
C
-3.40 mm
-3.64 mm
-3.88 mm
D
mCherry
100 µm
TH
-3.40 mm
Merge
VTA
IPR
ml
E
-3.40 mm
-3.64 mm
-3.88 mm
F
Speed (m/s)
Veh
CNO
G
Amount eaten (g)
SC
CP
H
Baseline
Onset
AUC
SC
CP
Tail
I
Baseline
Onset
AUC
SC
CP
Tail
J
SC
CP
2 z-scores
5 s
K
Tail
2 z-scores
5 s
L
Speed (m/s)
mCherry
hM4D-mCherry
Veh
J60
M
Speed (m/s)
Water
Cat urine
Veh
J60

Figure S2. VTA-VGluT2 neurons signal innate escape responses, related to Figure 2. (A) Diagram of VTA viral injection of AAV-Flex-GCaMP6s and VTA photometry fiber. **(B)** Detection of VTA-VGluT2 neurons expressing GCamP6s-GFP (green) below the photometry fiber. **(C)** Placement of photometry fibers within the VTA (red, looming and odor experiments; yellow, feeding and tail grab experiment). **(D)** VTA detection of VGluT2 neurons (mCherry, red) and TH neurons (green). **(E)** VTA rostral to caudal extension of hM4D-mCherry viral injections indicating maximal (red) and minimal (pink) diffusion. (**F**) Maximum speed of hM4D-mCherry mice was not modified by intraperitoneal administration of CNO during TMT odor presentation ($t_{(24)}$=-1.88, P=0.07, *t* test; data represent means ± SEM). (**G**) The amount of food eaten was significantly higher when chocolate-flavored sucrose pellets (CP) were presented to the mice instead of standard chow (SC: n=9; $t_{(16)}$=-2.58, * P<0.05, *t* test; data represent mean ± SEM). (**H**) Individual values of area under the curve (AUC) for Ca^{2+} activity in VTA-VGluT2 neurons before (-5s – 0s, baseline) and after (0s – 5s, onset) the onset of food consumption or tail grab. (**I**) AUC for Ca^{2+} activity in VTA-VGluT2 neurons in response to SC, CP or tail grab (n=9; event x epoch: $F_{(2, 24)}$=4.40, P<0.05, ANOVA with Newman-Keuls *post hoc* test. *** P<0.001 against onset for the same event; + P<0.05, ++ P<0.01 against tail grab onset; data represent mean ± SEM). (**J**) Population Ca^{2+}activity (± SEM) in VTA-VGluT2 neurons during the onset of feeding. (**K**) Population Ca^{2+}activity (± SEM) in VTA-VGluT2 neurons during the onset of the tail grab and lift. (**L**) Maximum speed was not modified by intraperitoneal administration of J60 during TMT odor presentation (group x drug: $F_{(1,10)}$=0.20, P=0.67, ANOVA; data represent mean ± SEM). (**M**) Maximum speed was not modified by intra-VTA administration of J60 during cat urine or water presentation (odor x drug: $F_{(1,15)}$=0.05, P=0.83, ANOVA; data represent mean ± SEM).

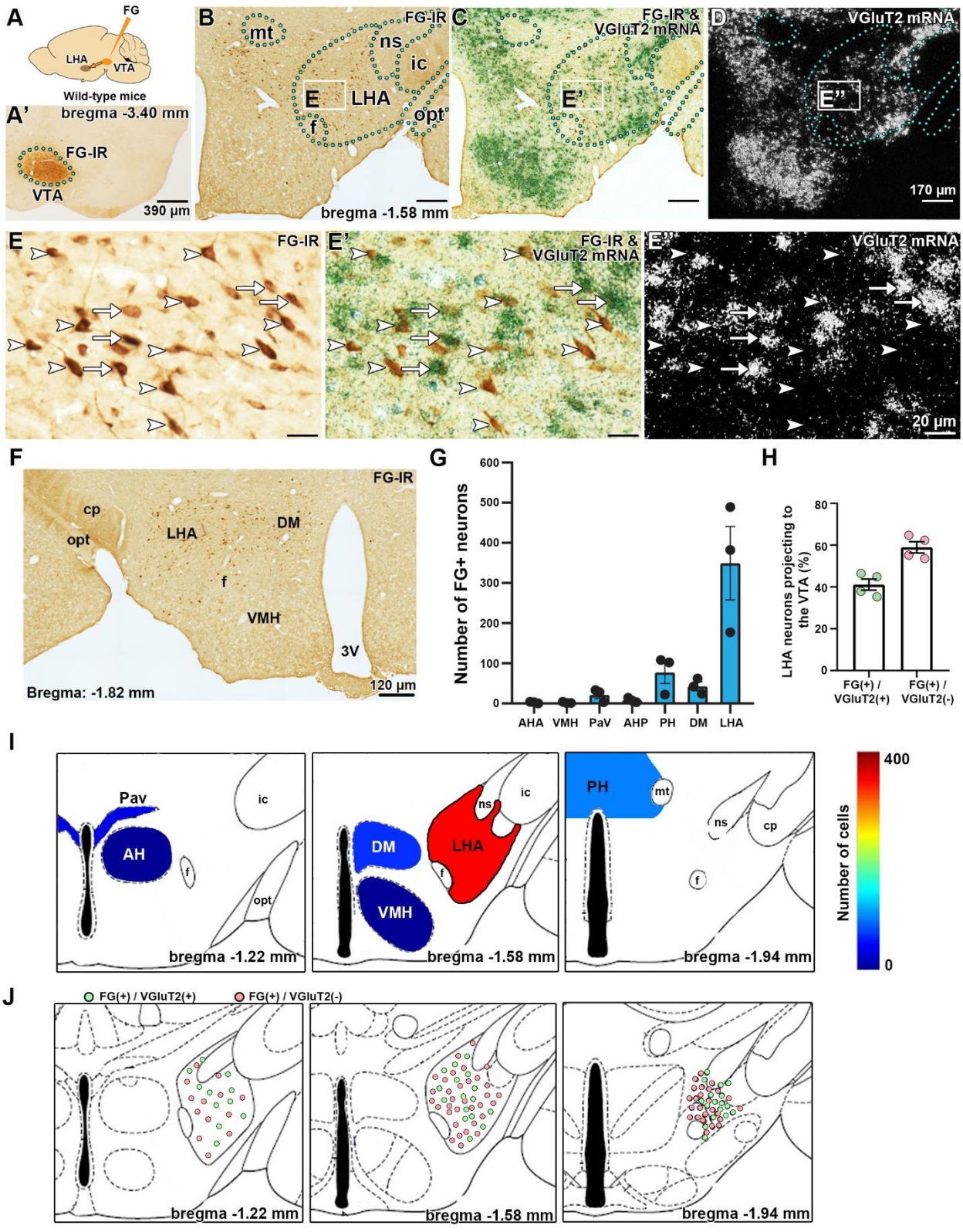

Figure S3. LHA neurons expressing VGluT2 mRNA provide a major input to VTA, related to Figure 3. (**A**) VTA iontophoretic application of the retrograde tracer Fluoro-Gold (FG) (**A'**) FG-immunoreactivity

(FG-IR) in VTA. (**B-D**) Low magnification of LHA showing retrogradely FG-IR (brown, **B**), and expression of VGluT2 mRNA under brightfield-epiluminiscence microscopy (green aggregated grains, **C**) and under epiluminiscence microscopy (white aggregated grains, **D**). (**E-E"**) Square areas in **B-D** are shown at higher magnification. Retrogradely FG-IR neurons co-expressing (arrows) or lacking VGluT2 mRNA (arrowheads). (**F**) Photomicrograph of retrogradely FG-IR neurons in the LHA and adjacent hypothalamic subregions. (**G**) Quantification of FG-IR neurons across the antero-posterior extent of the LHA and adjacent hypothalamic subregions following VTA iontophoretic application of FG (n=3). Most FG-IR neurons are located within the LHA, and fewer are in the anterior hypothalamic area, anterior part (AHA), ventromedial hypothalamic nucleus (VMH); paraventricular hypothalamic nucleus, ventral part (PaV), anterior hypothalamic area, posterior part (AHP), posterior hypothalamic area (PH) and dorsomedial hypothalamic nucleus (DM). Data represent mean ± SEM. (**H**) LHA frequency of FG-IR neurons expressing or lacking VGluT2 mRNA (n=4; data represent mean ± SEM). (**I**) Schematic heatmaps showing the average number of neurons projecting to the VTA within the hypothalamic subnuclei. (**J**) LHA distribution of FG-IR neurons co-expressing (green dots) or lacking (pink dots) VGluT2 mRNA. 3V, third ventricle; cp, cerebral peduncle; f, fornix; ic, internal capsule; LHA, lateral hypothalamic area; mt, mammillothalamic tract; ns, nigrostriatal bundle; opt, optic tract; VTA, ventral tegmental area.

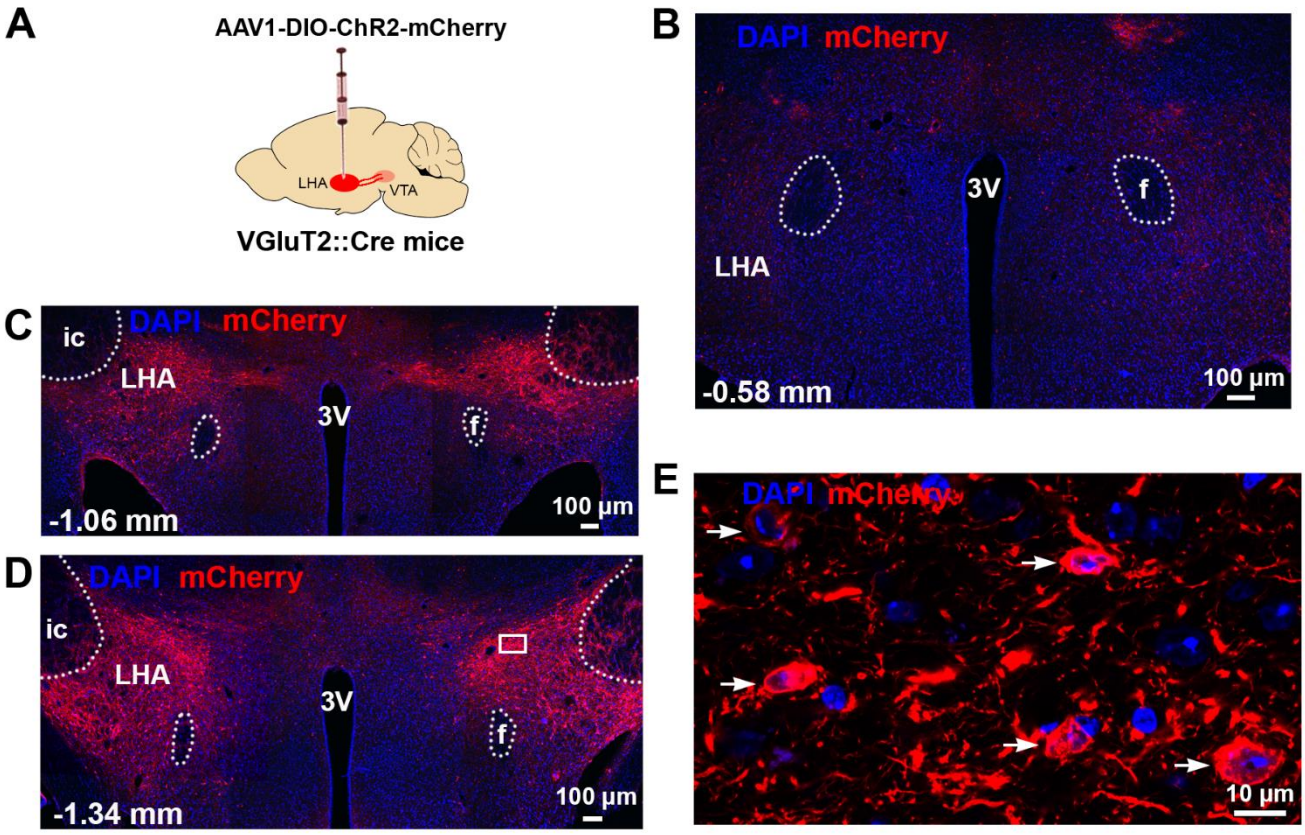

Figure S4. Detection of viral injection sites (mCherry) at the rostro-caudal level of the LHA, related to Figure 3. (**A)** Diagram of LHA viral injections of ChR2-mCherry. (**B-D**) LHA images showing the rostro-caudal extension of viral injections at low magnification. (**E**) LHA-VGluT2 transfected neurons (box in **D**) are seen at higher magnification (white arrows).

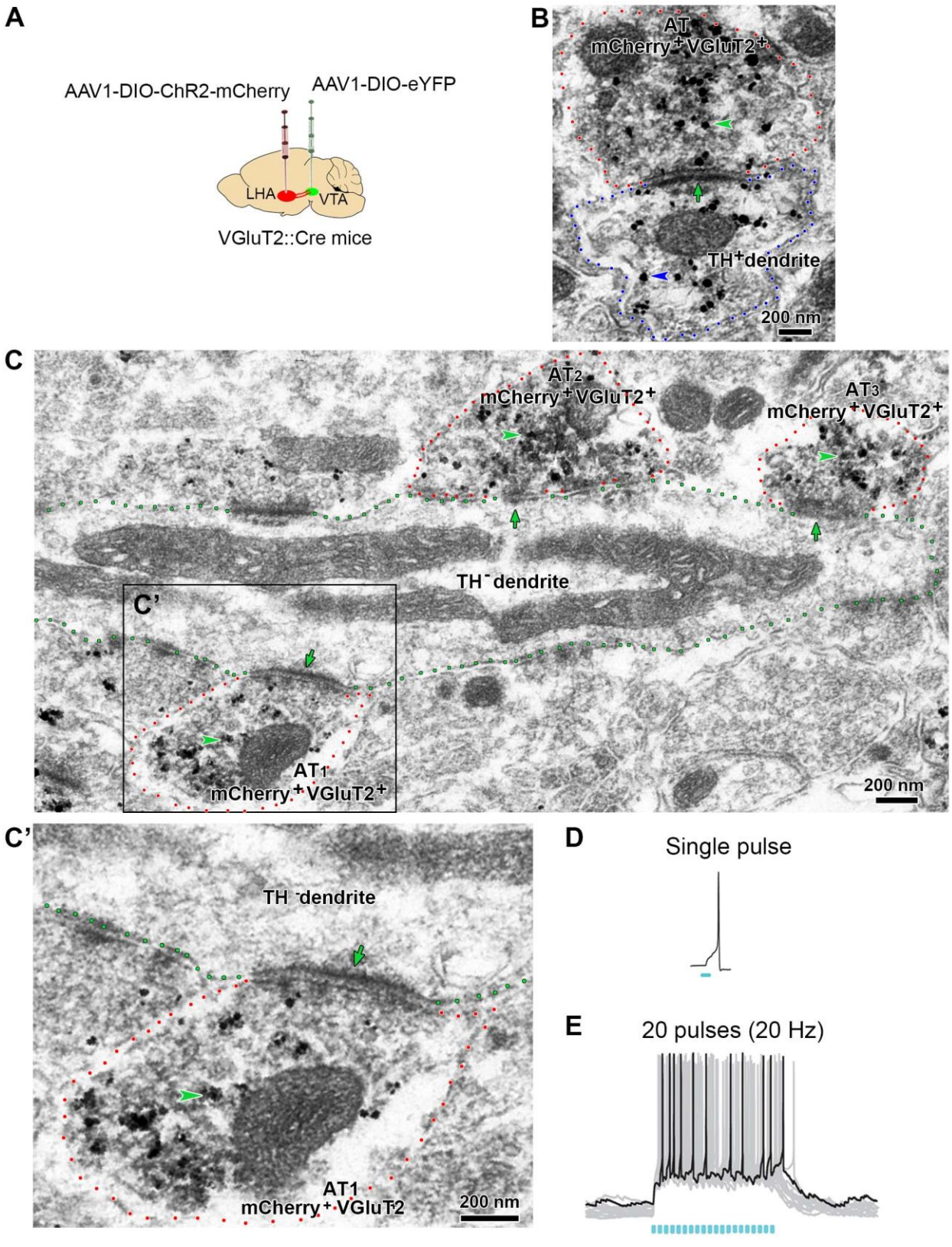
A
AAV1-DIO-ChR2-mCherry
AAV1-DIO-eYFP
LHA
VTA
VGluT2::Cre mice
B
AT
mCherry+VGluT2+
TH+dendrite
200 nm
C
AT2
mCherry+VGluT2+
AT3
mCherry+VGluT2+
TH- dendrite
C'
AT1
mCherry+VGluT2+
200 nm
C'
TH- dendrite
AT1
mCherry+VGluT2
200 nm
D
Single pulse
E
20 pulses (20 Hz)

Figure S5. LHA-VGluT2 neurons make asymmetric synapses on both VTA-dopamine and non-dopamine neurons, related to Figure 3. (**A**) Diagram of viral injection of AAV1-DIO-ChR2-mCherry into LHA and AAV1-DIO-eYFP into VTA of VGluT2::Cre mice. (**B**) An axon terminal (AT, red outline) from a LHA-VGluT2 neuron co-expressing mCherry (scattered dark material) and VGluT2 (green arrowhead, gold particles) makes an asymmetric synapse (green arrow) on a VTA-TH (blue arrowhead, gold particles) dendrite (blue outline). (**C**) Low magnification image showing a VTA-TH negative dendrite (green outline) makes asymmetric synapses (green arrows) with three axon terminals (AT_{1-3}, red outline) from LHA-VGluT2 neurons co-expressing mCherry (scattered dark material) and VGluT2 (arrowhead, gold particles). (**C'**) Higher magnification image from **C** showing an axon terminal (AT, red outline) from an LHA-VGluT2 neuron co-expressing mCherry and VGluT2 that makes an asymmetric synapse (green arrow) on a VTA TH-negative dendrite (green outline). (**D**) A single pulse of photoactivation of LHA-VGluT2 fibers evoked a single action potential in VTA-VGluT2 neurons. (**E**) Individual (gray) and averaged (black) current clamp traces from VTA-VGluT2 neurons during 1 s photostimulation (20 Hz) of LHA-VGluT2 fibers induced burst firing.

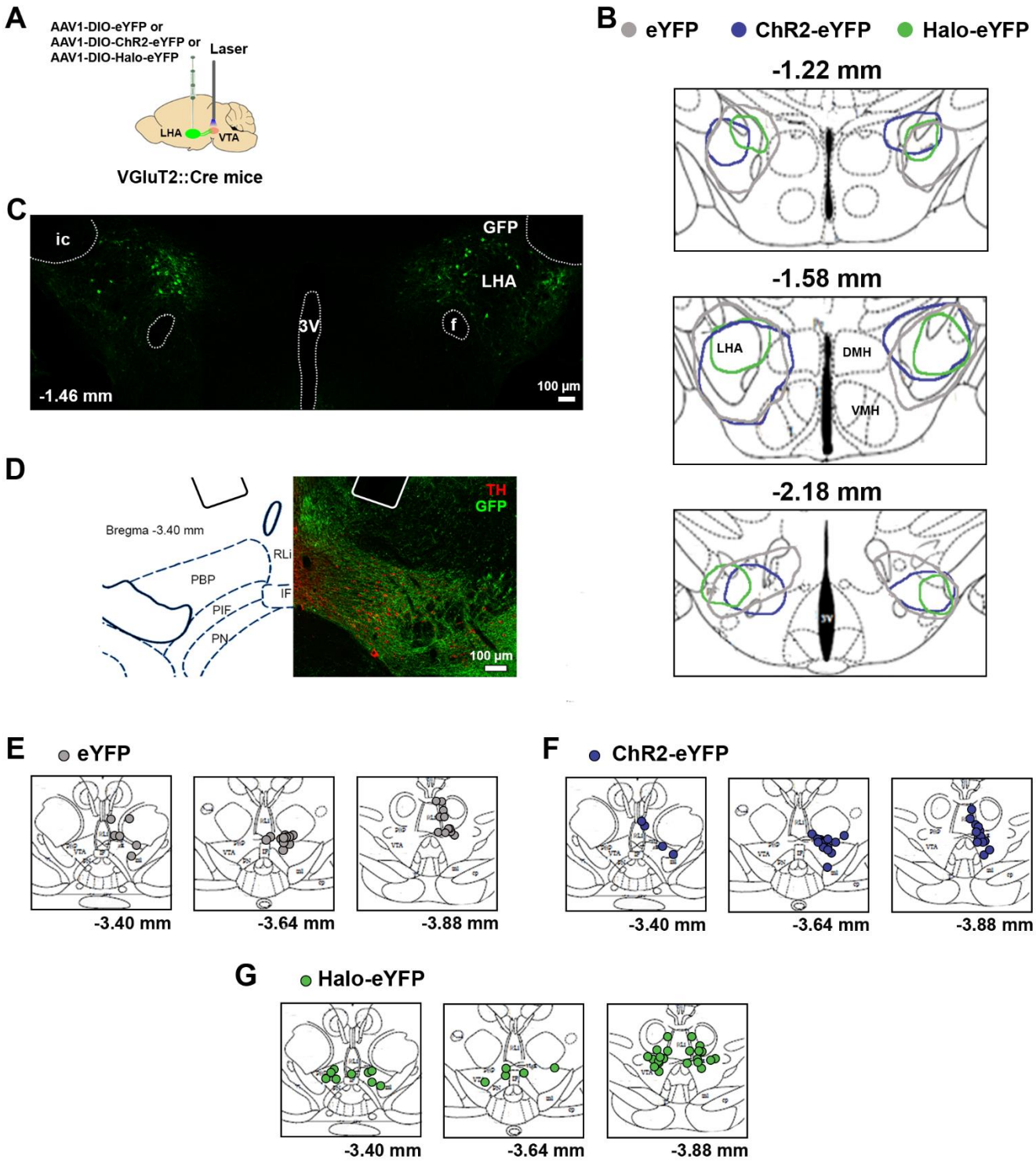

Figure S6. VTA photostimulation or photoinhibition of LHA-VGluT2 fibers modulates innate escape responses, related to Figures 4 and 5. (**A**) Diagram of LHA viral injections and VTA photostimulation of LHA-VGluT2 fibers. (**B**) Rostro-caudal extension of viral injections (eYFP, ChR2-eYFP and Halo-eYFP) within the LHA. (**C**) Expression of Halo-eYFP (green) in LHA neurons. (**D**) VTA optic fiber placements

and detection of eYFP fibers from LHA-VGluT2 neurons (green) and TH (red). (**E)** Optic fiber placements in eYFP mice. (**F**) Optic fiber placements in ChR2-eYFP mice. (**G**) Optic fiber placements in Halo-eYFP mice.

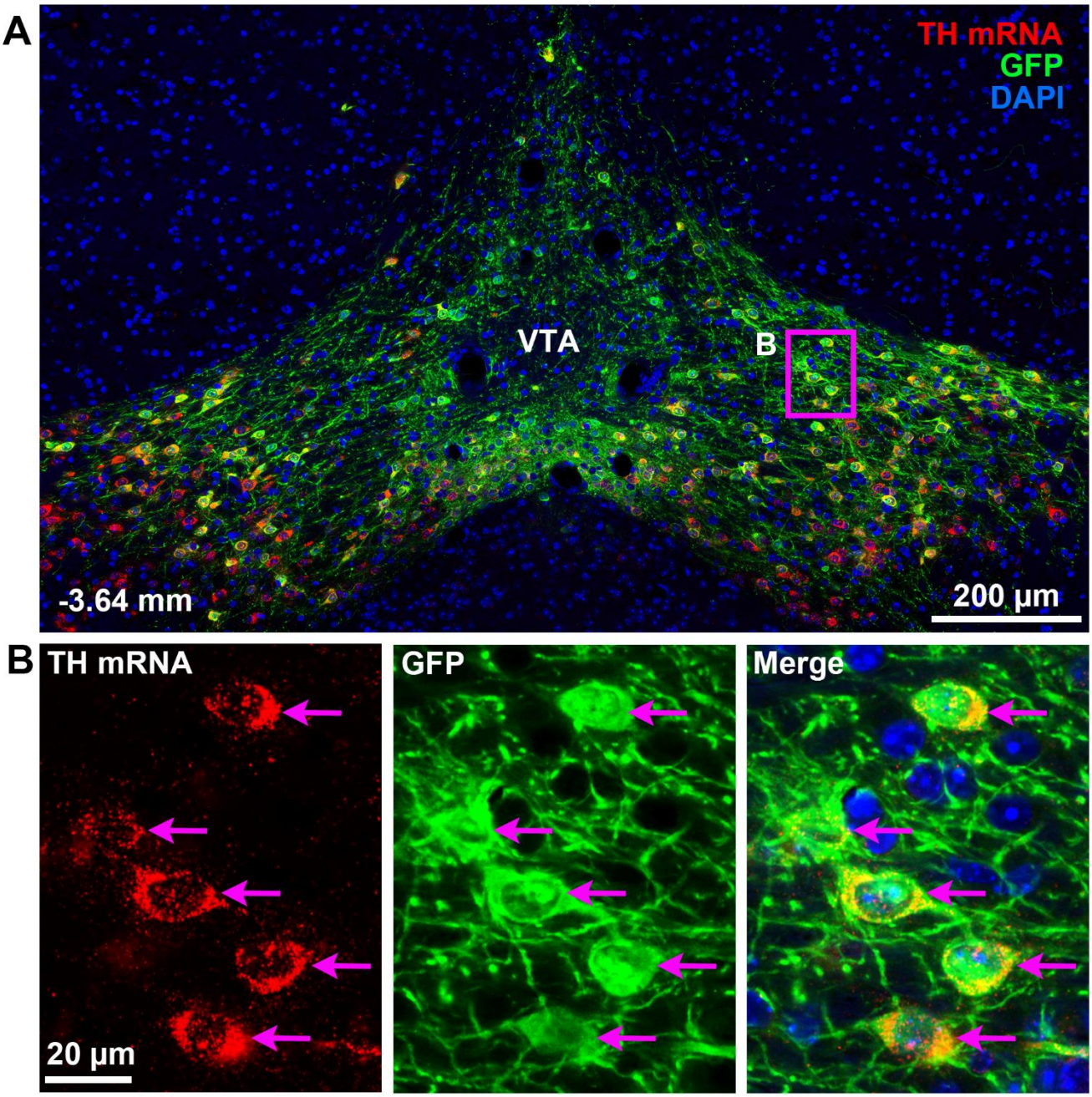

Figure S7. eYFP expression is restricted to VTA-TH neurons in TH::Cre mice, related to Figure 4. Low (**A**) and high (**B**) magnification of VTA from a TH::Cre mouse, injected with AAV1-DIO-eYFP, showing neurons expressing TH mRNA (red) intermixed with eYFP immunoreactive neurons (GFP, green). All eYFP positive neurons also co-expressed TH mRNA.

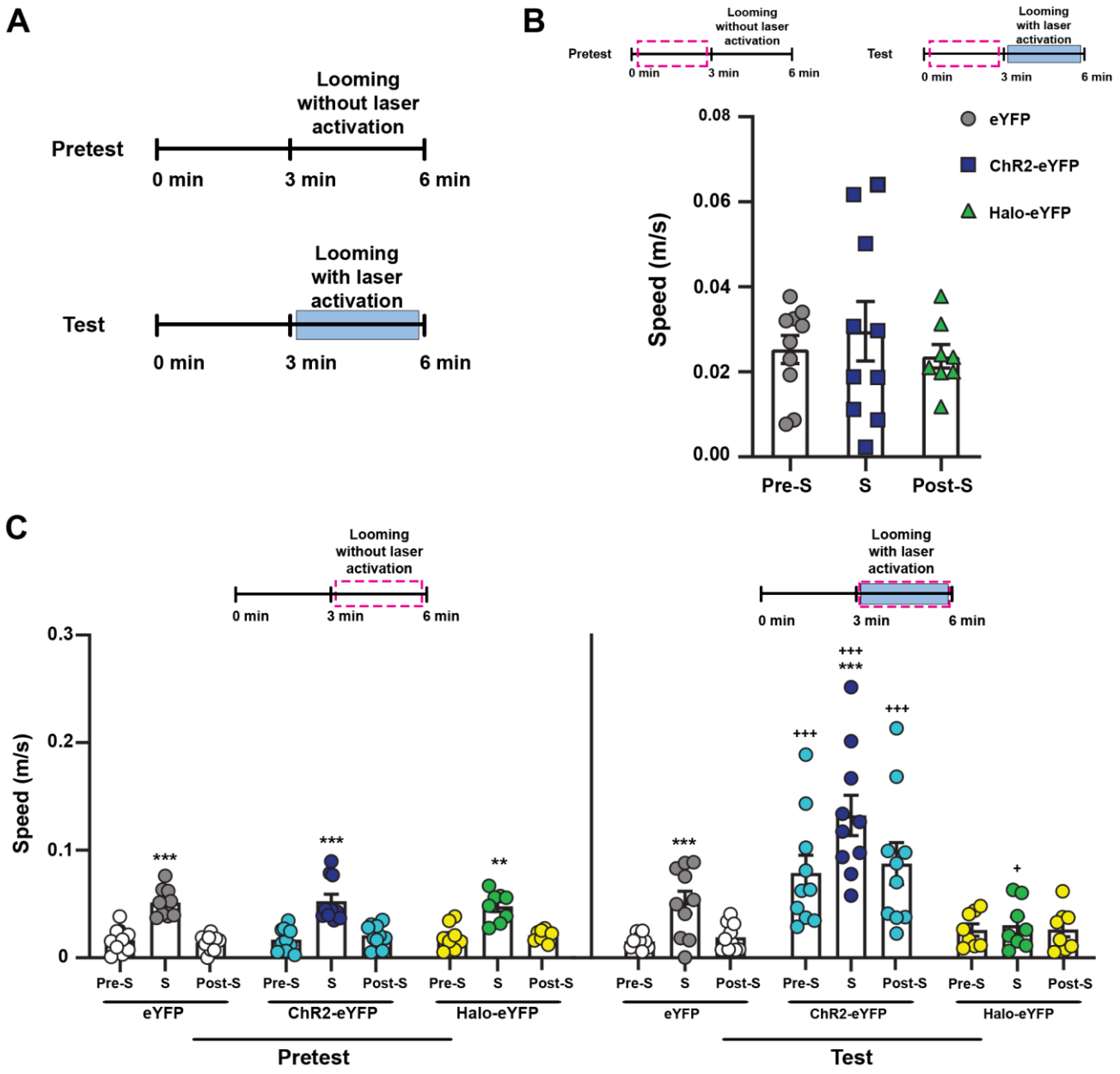

Figure S8. Speed analysis of mice confronted with a looming stimulus mimicking a predator, related to Figure 5. (**A**) Diagram showing the experimental design. Each phase of the test was divided in 10-s trials and the exact moment the looming stimulus was above the arena was calculated and assigned to its corresponding 10-s trial (stimulus trial, S). The speed during that 10-s trial, as well as the 10-s trials before (pre-stimulus trial, Pre-S), and after (post-stimulus trial, Post-S) was calculated for each mouse. The pink box in the next panels indicates in which phase the speed was measured. (**B**) The average speed of eYFP (n=10), ChR2-eYFP (n=10) and Halo-eYFP (n=8) mice did not differ during the first 3 minutes of either pretest or test (when no stimulus was presented, $F_{(2, 25)}$=0.37, P=0.69, ANOVA; data represent mean ± SEM). (**C**) Through pretest, the average speed was significantly higher during the 10-s trial in which the looming stimulus was presented (S) than during the previous (Pre-S) or subsequent (Post-S) 10-s trial for all the mice (main effect epoch: $F_{(2, 50)}$=96.90, P<0.001, ANOVA with Newman-Keuls *post hoc* test. ** P<0.01; *** P<0.001 against Pre-S or Post-S). Through test, the average speed of ChR2-eYFP mice was

significantly higher than the speed of eYFP mice during Pre-S, S and Post-S, while the speed of Halo-eYFP was decreased during S (group x epoch: $F_{(4, 50)}$=3.95, P<0.01, ANOVA with Newman-Keuls *post hoc* test. *** P<0.001 against Pre-S or Post-S; + P<0.05, +++ P<0.001 against the same trial within pretest; data represent mean ± SEM).

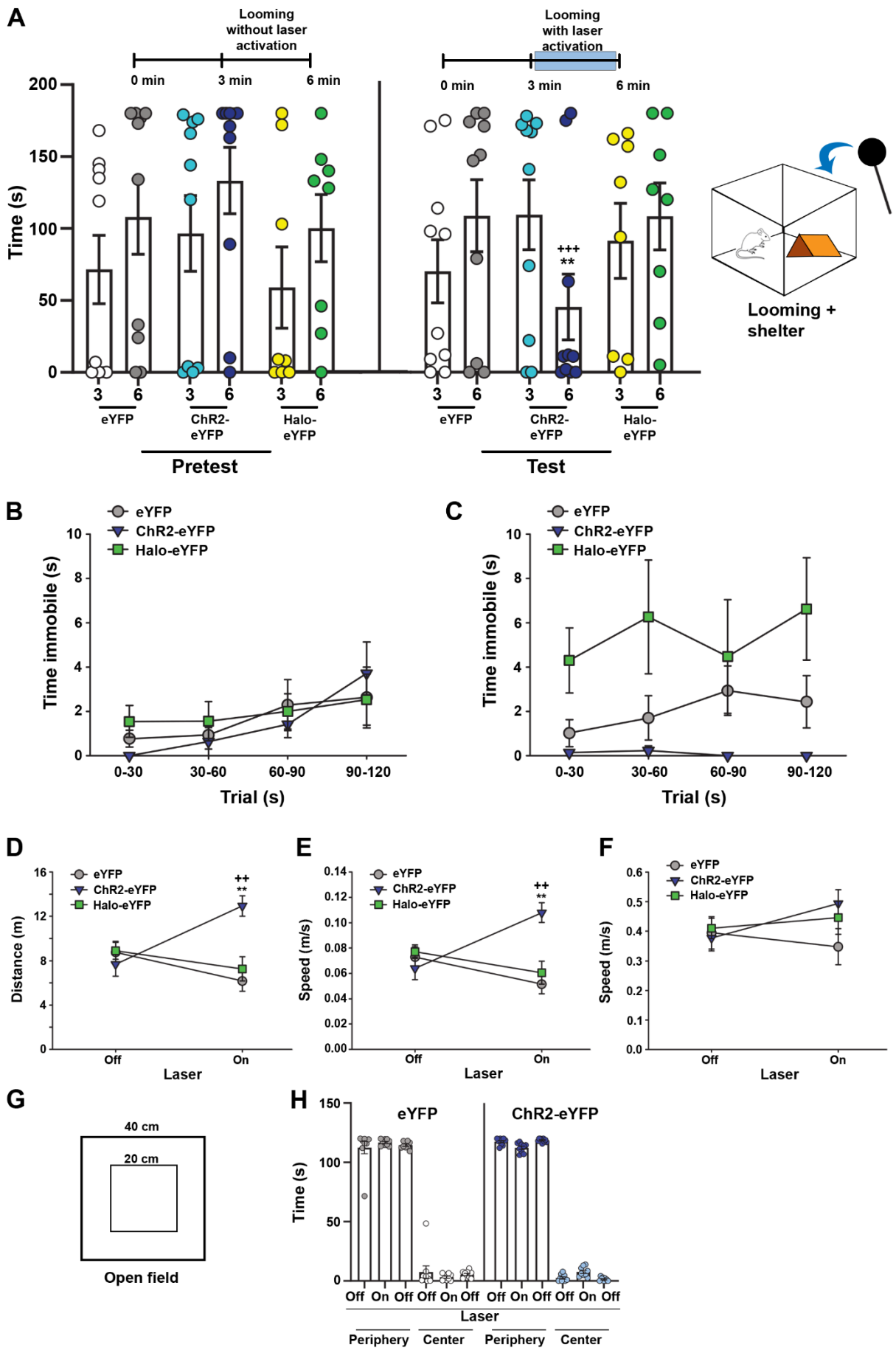
A
Looming without laser activation
Looming with laser activation
0 min
3 min
6 min
Time (s)
eYFP
ChR2-eYFP
Halo-eYFP
Pretest
Test
+++
**
Looming + shelter
B
C
Time immobile (s)
Trial (s)
0-30
30-60
60-90
90-120
D
E
F
Distance (m)
Speed (m/s)
Off
On
Laser
++
**
G
40 cm
20 cm
Open field
H
Periphery
Center

Figure S9. Time in shelter and forced swimming during VTA photostimulation or photoinhibition of LHA-VGluT2 fibers, related to Figure 5. (A) Time hiding from a looming stimulus during VTA photostimulation or photoinhibition of LHA-VGluT2 fibers in the presence of a shelter. In the absence of laser activation, mice from all groups spent similar amount of time hided in the shelter. Laser activation induced a decrease in the time hiding only in ChR2-eYFP mice (eYFP, n=10; ChR2-eYFP, n=10; Halo-eYFP, n=8; group x experimental phase x time: $F_{(2,25)}$=3.61, P<0.05, ANOVA with Newman-Keuls *post hoc* test; data represent mean ± SEM). ** P<0.01, against the first 3 min of the experiment, for each group; +++ P<0.001, against the same period in the pretest phase. **(B)** Total time immobile per trial before VTA photostimulation or photoinhibition of LHA-VGluT2 fibers. The time immobile was similar between groups (eYFP, n=9; ChR2-eYFP, n=9; Halo-eYFP, n=9; group: $F_{(2,26)}$=0.20, P=0.82, ANOVA with Newman-Keuls *post hoc* test; data represent mean ± SEM). **(C)** Total time immobile per trial during VTA photostimulation or photoinhibition of LHA-VGluT2 fibers (eYFP, n=9; ChR2-eYFP, n=9; Halo-eYFP, n=9; group: $F_{(2,26)}$=4.69, P<0.05, ANOVA with Newman-Keuls *post hoc* test; data represent mean ± SEM). **(D)** Increases in total distance swam during VTA photostimulation by ChR2-eYFP mice, but not by eYFP or Halo-eYFP mice (eYFP, n=9; ChR2-eYFP, n=9; Halo-eYFP, n=9; group x experimental phase: $F_{(2,26)}$=10.77, P<0.001, ANOVA with Newman-Keuls *post hoc* test; data represent mean ± SEM). **(E)** Only ChR2-eYFP mice significantly increased their average speed during VTA photostimulation (eYFP, n=9; ChR2-eYFP, n=9; Halo-eYFP, n=9; group x experimental phase: $F_{(2,26)}$=12.59, P<0.001, ANOVA with Newman-Keuls *post hoc* test; data represent mean ± SEM). **(F)** Maximum speed during forced swim test was not modified by VTA photostimulation or photoinhibition (eYFP, n=9; ChR2-eYFP, n=9; Halo-eYFP, n=9; group x experimental phase: $F_{(2,26)}$=1.69, P=0.20, ANOVA with Newman-Keuls *post hoc* test; data represent mean ± SEM). ** P<0.01, against eYFP; ++ P<0.001, against laser off. (**G**) Anxiety was measured in an open field arena. (**H**) Total time spent in the periphery and center zones before, during and after 20 Hz VTA photostimulation of LHA-VGluT2 fibers (eYFP, n=9; ChR2-eYFP, n=9; group x area x experimental phase: $F_{(2,32)}$=2.35, P=0.10, ANOVA with Newman-Keuls *post hoc* test; data represent mean ± SEM).

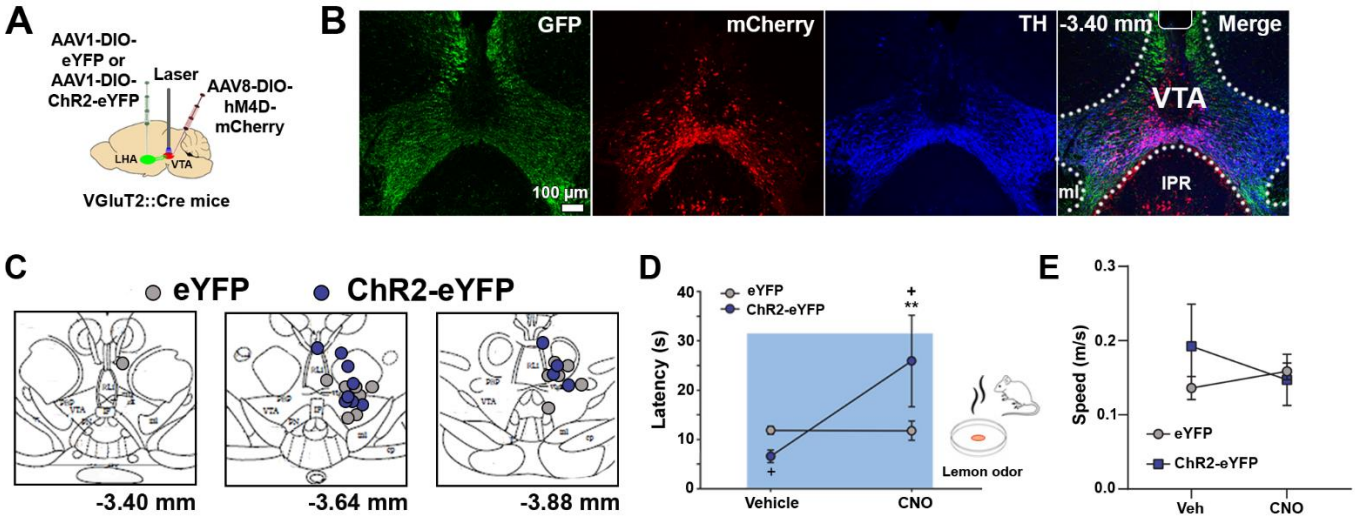

Figure S10. LHA-VGluT2 neurons projecting to VTA signal perceived threats, related to Figure 6. (**A**) Diagram of viral injections of AAV-DIO-ChR2-eYFP or AAV-DIO-eYFP in LHA and of AAV-hM4Di-mCherry in the VTA of VGluT2::Cre mice, and VTA photostimulation of LHA-VGluT2 fibers. (**B**) VTA detection of eYFP fibers from LHA-VGluT2 neurons (green), mCherry VGluT2 neurons (red) and TH neurons (blue). (**C**) Placement of optic fibers. (**D**) Latency to escape lemon odor in ChR2-eYFP (n=12) or eYFP (n=13) mice after VTA photostimulation of LHA-VGluT2 fibers (group x treatment: $F_{(1,23)}$=4.55, P=0.05, ANOVA with Newman-Keuls *post hoc* test; data represent mean ± SEM). ** P<0.01, against vehicle; + P<0.05, against eYFP. (**E**) Maximum speed was not modified by intraperitoneal administration of DREADD ligand CNO during lemon odor presentation (group x drug: $F_{(1,23)}$=1.23, P=0.28, ANOVA; data represent mean ± SEM).